

**APPLICATION OF MAGNETIC AND ELECTRICAL GEOPHYSICAL
METHODS IN DELINEATING
AURIFEROUS STRUCTURES IN THE SEFWI BELT OF GHANA**

BY

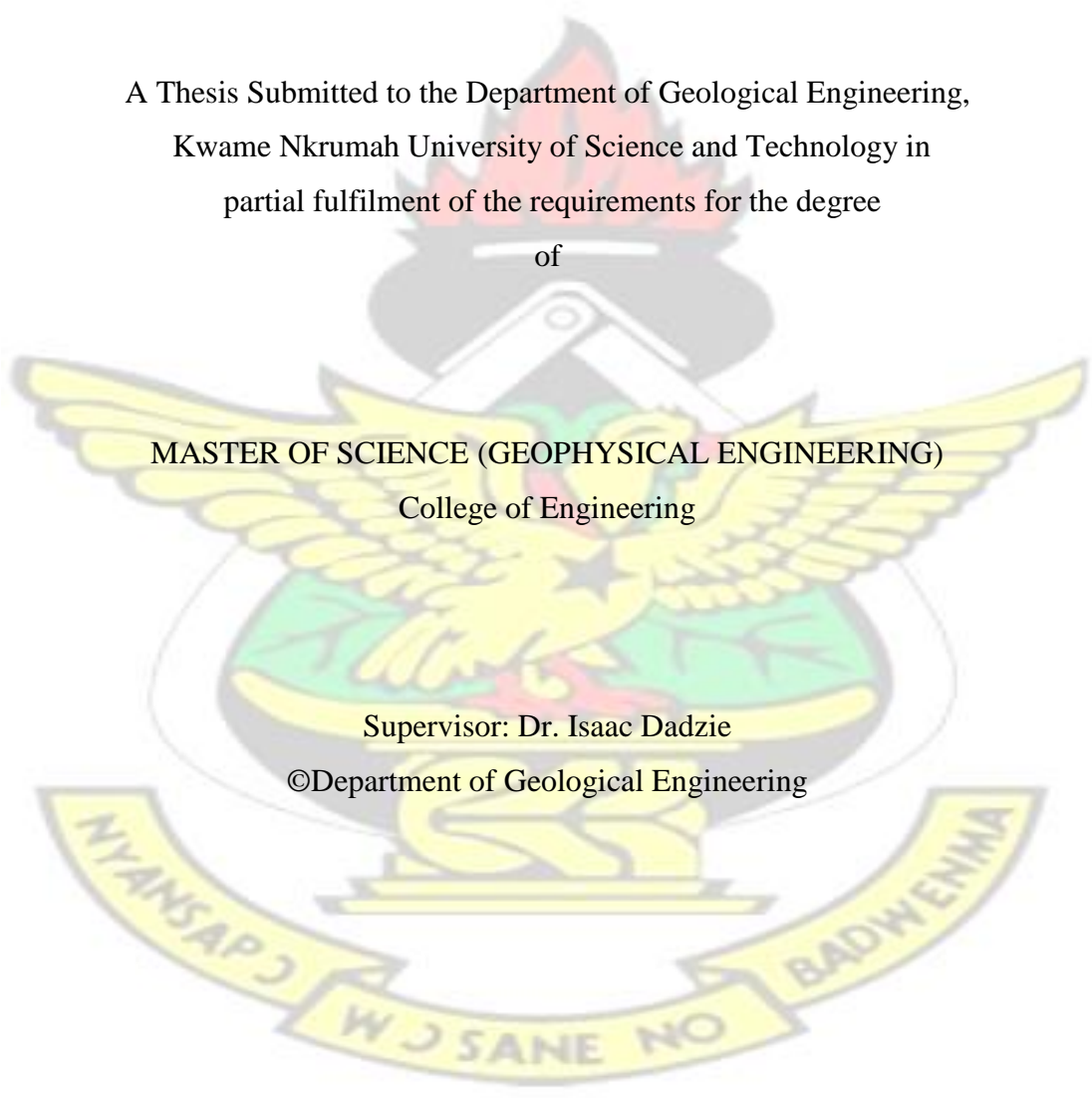
FAREED MAJEED, BSc Geological Engineering (Hons)

A Thesis Submitted to the Department of Geological Engineering,
Kwame Nkrumah University of Science and Technology in
partial fulfilment of the requirements for the degree
of

MASTER OF SCIENCE (GEOPHYSICAL ENGINEERING)
College of Engineering

Supervisor: Dr. Isaac Dadzie

©Department of Geological Engineering



OCTOBER, 2016

CERTIFICATION

I hereby certify that this thesis work is my own work as part of the requirements for the award of a Master of Science degree, and that it contains no material previously published by another person or material which has been accepted for the award of any other degree by the university, except where due acknowledgement has been made in the text.

KNUST

.....
Student's name & ID

.....
Signature

.....
Date

Certified by:

.....
Supervisor(s) Name

.....
Signature

.....
Date

.....
Supervisor(s) Name

.....
Signature

.....
Date

.....
Head of Dept. Name

.....
Signature

.....
Date

KNUST

DEDICATION

To Mum and Dad



ABSTRACT

Gold is a very important economic commodity to the growth of Ghana's development. The prospecting and exploration stages of mining involve long periods of investment with a high risk of failure. Even before strenuous effort is put into the discovery of reserves, many exploration companies become cash-strapped to the extent of collapse and may find near mine development very challenging. For this reason prospecting for gold needs to be optimized and that calls to mind the attention of choosing the right techniques that will enhance the success of the exploration projects. Four indicative spatial features -shear (ductile) zones, favorable host rock units with fracture arrays, hydrothermal alterations and strongly deformed (brittle) or faults zone- were the driven force behind this research. Two geophysical methods namely ground magnetic and electrical tools were integrated with existing geological dataset to map out structures in the Sefwi belt of Southern Ghana. The magnetic data obtained were processed into grids with Geosoft. Data enhancement filters such as reduction to the pole, tilt-angle derivative, first and second vertical derivatives and continuation filters were further applied to Total Magnetic Intensity (TMI) grid to enhance magnetic anomalies. The induced polarization-chargeability data were measured in the time domain. The positive anomalies on the IP-chargeability map coincided with the shears margins alterations and contact zones. Two dipole-dipole sections were carried out in the study area and were inverted using the RES2DINV program. From the results obtained, an interpreted definitive geologic map of the study area consisting of the geology, structures and hydrothermally altered zones were produced with MapInfo (Discover). All recognizable features were mapped as major and inferred thrust fault, lineation and alteration. The result is a preliminary mineral potential map.

The outcome of electrical resistivity and IP inversions indicated that depths ranging from 50 to 200 m suggests conductive and chargeable bodies. The low-resistivity

zones coincided with sheared and altered acidic meta-sediments. The geophysical signatures obtained from the enhanced magnetic data and the electrical data showed that the study area is structurally complex with a few of the structures corresponding to D1 deformation and most structures corresponding to D2 deformation. The lithostructures were interpreted as, meta-volcano sedimentary and belt granitoid units with varying discontinuities and lineation. According to the geophysical data integrated, seven suggested drill-hole sites were selected for definitive studies. The high resolution integrated geophysical study resulted in better definition of both geologic structures and lithological boundaries. This work shows the worth of geophysical data as an enhancement tool in mapping possible geologic structures that host hydrothermal gold mineralization within the Sefwi Gold belt of Ghana.



ACKNOWLEDGEMENTS

My heartfelt appreciation goes to my supervisor, Dr. Isaac Dadzie for his immeasurable support and direction offered to the success of this thesis. No words can express my indebtedness to my co-supervisor, Mr. Kweku Tekyi-Kyeremeh for providing the data for this work and painstakingly addressing all critical issues therein. Without them, I could not have completed this research.

I would like to express my profound gratitude to Professor F. Boadu for his advice well-spoken encouragement. To the head of department Professor S.K.Y Gawu, Mr. Gordon Foli and the entire staff of the Geological engineering department, I say thank you for making the department a wonderful home to the success of the project.

To all the folks and first batch of MSc. Geophysical engineering, I say thank you for your patience and tolerance during the period of our studies. Special thanks also go to Mr. Nana Kena Frimpong and Dr. Ayekple of department of Mathematics, KNUST for their hospitality and encouragement.

I am also indebted to my wonderful siblings, Issah, Saeed, Omolola, Mubarak, Omoshola and Tawfeeq Afedzi Majeed, whose prayers and absolute trust proved to be like a bulwark in times of anxiety and worthlessness. Most especially to my lovely wife, Joycelyn Abena Krakue Sejesar, I say thank you for your prayers, love and utmost trust in me that was a source of comfort and encouragement.

Ultimately, my absolute appreciation and honour goes to the Grand Creator and sustainer of life, Jehovah God, who gave me the strength and fortitude to endure, persevere and complete this task.

TABLE OF CONTENTS

CERTIFICATION	ii
DEDICATION	iii
ABSTRACT.....	iv
ACKNOWLEDGEMENTS	v
TABLE OF CONTENTS.....	vii
LIST OF TABLES	xi
LIST OF FIGURES	xii
LIST OF ABBREVIATIONS AND ACRONYMS	xii
CHAPTER ONE	1
INTRODUCTION	1
1.1. Background.....	1
1.2. Research Problem Definition.....	5
1.3. Aims and Objectives	6
1.4. Justification.....	7
1.5. Scope of work and expected outcome	8
1.6. Structure of Thesis	8
CHAPTER TWO	10
LITERATURE REVIEW	10
2.1 Regional geology and structural setting.....	10
2.2. Types of gold occurrences	11
2.2.1. Birimian-Hosted Deposits.....	12
2.2.2. Intrusive Related Deposits	12
2.2.3. Tarkwaian (Paleoplacers) Hosted Deposits	13
2.3. Gold belts of Ghana	13
2.3.1. The Sefwi belt.....	14
2.4. Local Geology and Gold mineralization.....	17
2.5. Project Area	17
2.6. Accessibility.....	18
2.7. Climate and Vegetation	19
2.8. Setting of Study Area.....	19
CHAPTER THREE	21
THEORETICAL BACKGROUND.....	21
3. Ground magnetic.....	21

3.1.1. Introduction.....	21
3.1.2. Basic Concept	21
3.1.3. Magnetic Susceptibility	22
3.1.4. Rock magnetization	24
3.1.5. Diamagnetism, Paramagnetism and Ferromagnetism	25
3.1.5.1. Diamagnetism	25
3.1.5.2. Paramagnetism.....	25
3.1.5.3. Ferromagnetism	25
3.1.6. The Curie temperature	26
3.1.7. Remanent Magnetism	26
3.1.8. Principle of Magnetic method.....	27
3.1.9. Magnetic anomalies	28
3.1.10. Magnetic survey instruments	31
3.1.10.1. Magnetic balance	31
3.1.10.2. Flux-gate magnetometer	31
3.1.10.3. Proton precession magnetometer	32
3.1.11. Magnetic Survey Design and data acquisition.....	33
3.1.12. Data Reduction and Processing	33
3.1.13. Data presentation and enhancement	33
3.1.14. Magnetic data filtering.....	34
3.1.15. Qualitative interpretation	34
3.1.16. Quantitative interpretation	34
3.2. Electrical method	35
3.2.1. Introduction.....	35
3.2.2. Conduction in rocks	36
3.2.3. Electrical resistivity	36
3.2.3.1. Basic concept electrical method	37
3.2.3.2. Current flow in the ground.....	38
3.2.3.3. Survey design and data acquisition.....	40
3.2.4. Induced Polarization	41
3.2.4.1. Basic concept on induced polarization	42
3.2.4.2. Survey Design and measurements	44
3.2.5. Processing of Resistivity and IP Data.....	45
CHAPTER FOUR.....	46

METHODOLOGY FOR DATA ANALYSIS	46
4.1. Data Processing software	46
4.2. Data source	48
4.2.1. Ground Magnetic Metadata	48
4.2.1.1. Data Enhancement	49
4.2.1.2. Gridding	49
4.2.1.3. Magnetic data filtering	50
4.2.1.3.1. Upward-Continuation	50
4.2.1.3.2. Reduced to pole and equator	51
4.2.1.3.3. First vertical derivative	52
4.2.1.3.4. Tilt angle derivation	52
4.2.2. Gradient Resistivity and Induced Polarization	54
4.2.3. Gradient Resistivity / IP data processing	54
4.2.4. Gradient Resistivity / IP Qualitative map	55
4.2.5. Pole-dipole geoelectric section	55
4.2.6. Pole-dipole data processing	56
4.2.7. Pole-dipole Inverse model	56
4.2.8. Model Theory	57
4.2.9. Pole-dipole Quantitative map	58
CHAPTER FIVE	58
RESULTS AND DISCUSSIONS	58
5.1. Digital elevation map	58
5.2. Mapping of structural features	59
5.3. Qualitative Interpretation	60
5.3.1. Interpreting Lithological units	60
5.3.2. Structural interpretation	62
5.3.2.1. Pole-dipole Geoelectrical inversion	65
5.3.3. Extraction Alteration anomalies	67
5.4. Mineral potential map	68
CHAPTER SIX	70
CONCLUSION AND RECOMMENDATION	70
6.1. Conclusions	70
6.2. Recommendations	71
REFERENCES	72

APPENDICES 77
APPENDIX A 77
APPENDIX B 82
Used Software 82

KNUST



LIST OF TABLES

Table 2.1 Study area boundary pillars	17
Table 3.1 Common Rocks with their magnetic susceptibility values (Telford et al., 2004)	23
Table 3.2 Resistivities of rocks, minerals and chemicals adapted after Lowrie (1990)	36
Table 5.1 Proposed diamond drill holes.....	71



LIST OF FIGURES

Figure 2.1 Gold systems and crustal depths of emplacement. Adapted from Poulsen, 2000 and Robert, 2004a.	11
Figure 2. 2 Principal Gold belts of Ghana (Griffis et al, 2002)	16
Figure 2. 3 Regional map, Google location map and geological map (Griffis et al, 2002)	18
Figure 3.1 Hysteresis curve, Kearey et al., 2002.	27
Figure 3.2 Geomagnetic elements, modified after Kearey et al (2002). Representation vector geomagnetic field modified after Keary (2002).....	29
Figure 3.3 The horizontal (ΔH), vertical (ΔZ) and total field (ΔB) anomalies due to an isolated positive pole modified after Kearey et al (2002).	30
Figure 3.4 (a) Current flow from a single surface electrode (b) parameters used in defining resistivity	39
Figure 3.5 The phenomenon of IP, adapted from Kearey et al., (2002).	43
Figure 5.1: 3D surface DEM of study area	60
Figure 5.2 Interpreting lithological units from RTP magnetic anomaly	62
Figure 5.3 Tilt derivative and resistivity anomalous map	63
Figure 5.4: Tilt angle lineament (foliation) and 1 VD shear/foliation lineaments	65
Figure 5.6 Pole-dipole section Line 22700	67
Figure 5.7 Alteration anomalies mapped from IP chargeability and resistivity signatures	68
Figure 5.8 Interpreted detail geological and mineral potential map	70

LIST OF ABBREVIATIONS AND ACRONYMS

B	Total magnetic field
CRM	Chemical remnant magnetization

D Angle of declination

DEM Digital elevation map

DRM Detrital remnant magnetization

H Horizontal component of total magnetic field

H Magnetizing field strength

I Angle of inclination

IGRF International Geomagnetic reference Field

IP Induced polarization

IRM Isothermal remnant magnetism.

J Induce magnetization

K Magnetic susceptibility MSL Mean sea level nT Nano Tesla

RTP Reduced to pole

TMI Total magnetic intensity

TRM Thermoremnant magnetization

VES Vertical electrical sounding

VRM Viscous remnant magnetism

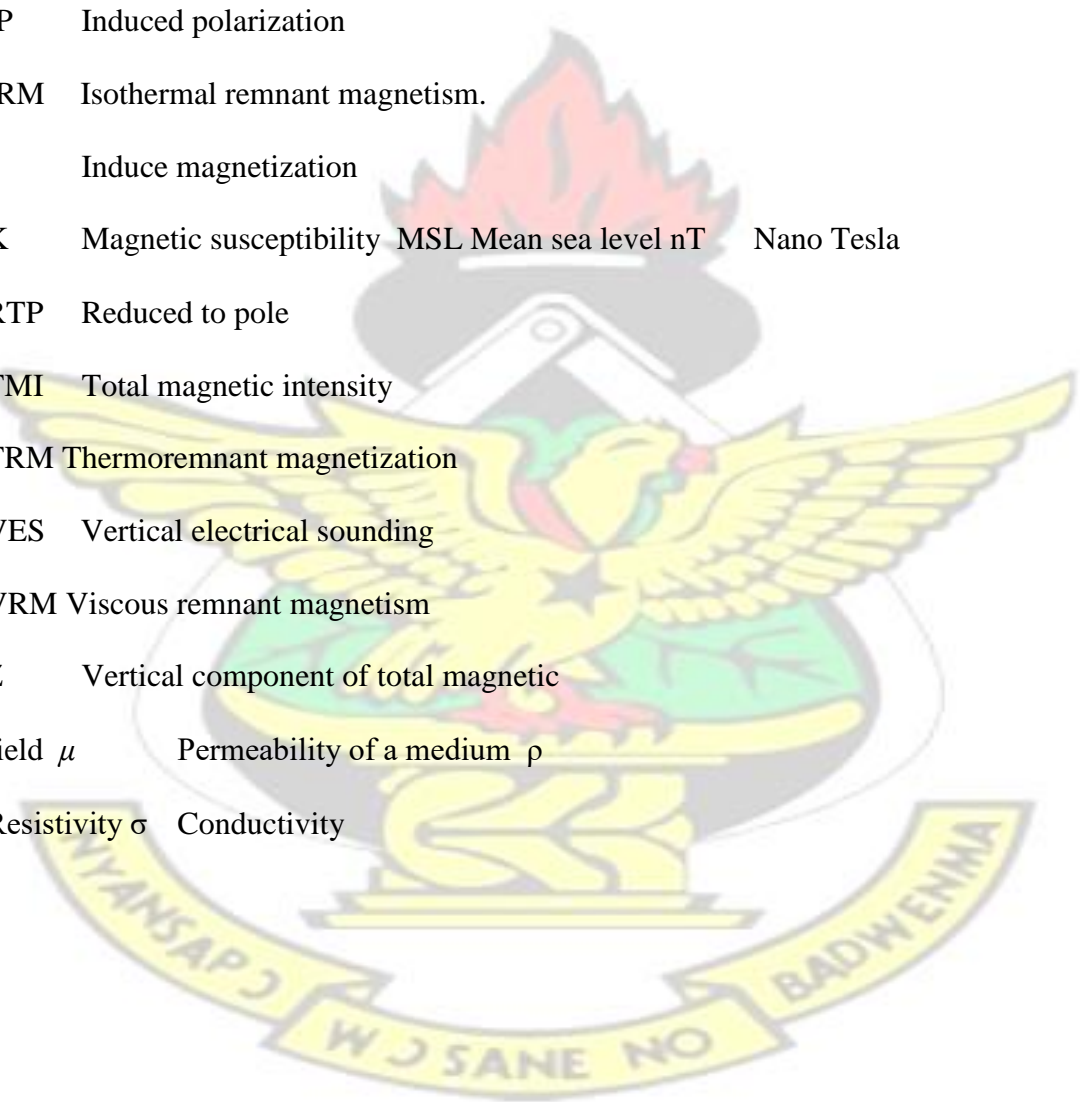
Z Vertical component of total magnetic field

μ Permeability of a medium

ρ Resistivity

σ Conductivity

KNUST



CHAPTER ONE

INTRODUCTION

1.1. Background

In Ghana, gold mining forms a major economic activity that has contributed tremendously to the socio-economic development of the country both in the past and present. Since the early days of mining to recent times, Ghana has been the hub for both exploration and mining investors due to its stable political and friendly mining jurisdiction. Africa and for that matter West Africa was a very significant gold producer for much of the past two millenniums. Much of the early production comes from the present day regions of Mali and Guinea whereas Akan states (Ghana and part of Ivory Coast) became more dominant by about 1400AD.

In the early 1900's, the then Gold Coast (now Ghana) emerged as an important new producing country on the world scene. The earliest form of gold exploration was nothing more than gathering free nuggets or gravity gold which the artisan in historic past popularly termed as "galamsey" carried from the expression "gather and sell". Griffis et al 2002 emphasized that gold mining has had a long history in the country and the quite dramatic increases in production in the 1990s have made gold the largest earner of foreign exchange in recent years.

Exploration is basically preoccupied with the tracking of known gold deposits and integration of a variety of tools with geology for their effective detection and quantification. It is the process of detail logical hypothesis building and testing so exploration strategy should be selected with huge amount of thoughts and research.

Exploration model may involve integration of geology, soil geochemistry, geophysics and structural signatures in defining potential gold deposits. It is noteworthy that none of these methods are “stand-alone” in gold prospecting.

Numerous research findings available on gold deposits in the last two decades have led to major improvement in the perception of models, definitive deposit types or subtypes and the emergence of new nomenclature. For example, gold mineralization is structurally controlled and is generally associated with shear zones, faults and fractures. It has long been established that structure is the key factor in controlling the lode gold deposits of Southern Ghana. From a current exploration viewpoint, one could rather superficially describe the three most important ore controls in the Southern belts of Ghana to be „Structures, structures and structures“ (Griffis et al., 2002). Common structural features such as thrust and strike-slip faults are basically associated with shear zones. They are commonly heated (between 7 and 12 km in depth) at or close to the transition from ductile to brittle regions in the crust (Heureux et al, 2007). Hydrothermal fluids cause changes in the adjacent rocks, resulting in mineralization. This phenomenon is often referred to as wall rock alteration (Fon et al., 2012). The adjacent rocks results in mineralogical changes which bring about major differences in physical properties of subsurface geologic units and they consequently display variable geophysical signatures (Fon et al., 2012).

General features of many gold deposits in the Southern in the Ashanti belt of Ghana are broadly hosted by Birimian meta-sediments and meta-volcanics with various mineralization vein and alteration styles. Certainly, from economic viewpoint, these are the most important types that have produced about 75% of the considerable production over the past century (Griffis et al., 2002).

The depth, size and geometry of structurally-hydrothermally controlled ore-bodies are defined by means of systematic drilling and subsequent 2D imagery of the drillhole stratigraphy. One key fact is that structures may host ore-bodies or deform them! However, prospecting and exploration stages of mining involves long periods of investments with a high risk of failure, hence a thorough, meticulous and systematic cost effective and optimum tool are needed to unravel it.

Many exploration projects have failed with its high cost and environmental impacts, from trenching, drilling (pad preparation). The old adage, failing to prepare is preparing to fail holds true in exploration industry. It may be prudent to conclude that investors have not favoured geophysics and/or exploration managers have not fully grasp or appreciated the concepts. Many companies, however, have resorted to geophysics at latter stages of prospecting or simply ignored it entirely. Initial stages of exploration project can make use of geologic and geophysical data for regional recognition of mineral trends. Over the years, Geographic Information System (GIS) techniques have been developed to grade and manage spatial data sets. Upon considerations of such datasets, potentially economic areas can be located and regional bedrock geology or major structural trends defined and delineated.

Induced Polarization geophysical method provides unique lithological information. It is also an excellent tool in areas predominant of quartz veins signatures with/and disseminated sulphides. Self-Potential (SP), gravimetric combined with IP and resistivity geophysical tools have been applied to the investigation of large hydrothermal systems, active volcanoes and large geological structures (Fon et al., 2012., Hase et al., 2005). The induced polarization-chargeability electrical field acquisition was measured in the time domain.

A gradient survey is a useful tool for covering a large area in which the positions of anomalies are not well known. Once a gradient survey has been completed and potential anomalous positions identified, then suitable lines can be selected to carry out detailed 2D surveys with multi-dipole or pole-dipole arrays.

Pole-dipole gives a unique 2-dimension vertical geo-electrical section of the subsurface. It has significantly high signal strength and relatively good horizontal coverage. It is less susceptible to telluric noise as other electrical array configurations, hence high signal-to-noise ratio.

The pole-dipole configuration is more efficient than the dipole-dipole array because it only involves the movement of only one transmitter electrode; hence it generates by far higher receiver voltages. The method involves the use of standard survey equipment involving sixteen fixed dipole receiver electrodes per set-up and a mobile pole current electrode. The use of copper electrode immersed in copper sulphate solution is essential for good electrical contact and reduce high contact resistance.

Magnetic survey is probably the oldest branch of geophysics. In exploration, acquisition of magnetic measurements is usually airborne, ground, on the ocean, in space, and down boreholes. It may cover a large range of scales and for a wide variety of purposes. Ground magnetics can provide a better perceptive of the bedrock geology and structures. Magnetic survey is a well-known technique to delineate subsurface structures and has been extensively used in many parts of the world. Magnetic susceptibility is the significant variable in magnetic survey. Sheriff (1928) noted that magnetic anomalies are caused by magnetic minerals (mainly magnetite and pyrrhotite) contained in rocks.

Most rock forming minerals are magnetized by induction in the Earth's field, and cause spatial perturbations or "anomalies" in the Earth's main field. Telford et al, 1976, emphasize that man-made objects such as iron or steel are highly magnetized and locally will cause compromised magnetic anomalies up to several thousands of Nano Tesla (nT). The magnetic technique involves measuring the amplitude measure of the magnetic field at distinct points. These regularly distributed points are along planned survey lines throughout the area of interest. The magnetic field was measured with a proton precision instrument with accuracy of 0.1 nT at a regular interval of 1m on 50 m traverse line interval. The traverse lines are perpendicularly oriented north-east to the general strike direction (base line) of the survey area.

1.2. Research Problem Definition

The primary objective of every mineral exploration is to locate ore of economic mineral deposit. Developing an exploration strategy, designing model and selection of optimum exploration methods have been given little attention over the years.

Many exploration projects resort to geophysical techniques at the "dying" stages of their ambitious mineral exploration program thereby unable to optimize the overall project. On the other hand, exploration project managers have not fully understood the use and importance of geophysics in enhancing the search for mineral deposits. It is for this reason that integrated geophysical methods have been undertaken in the study area to map the geology, structures and hydrothermal altered zones. The study area is situated on the second largest and potential auriferous deposits after the famous Ashanti belt.

The Sefwi belt is characterized by various forms of alterations types, complex mineralization styles and structural trends which require the exhaustive use of

geological, geophysical, geochemical and structural datasets in its ore model. However, to fully understand the deposit there is the need to succinctly integrate the right dataset in the discovery of mineral deposit. Since most exploration programmes are doomed to failure, it is imperative to select the optimum exploration tools in the pursuit for economic mineral deposits of interest. It is in this wise that the integration of ground magnetic and IP (Resistivity and chargeability) is used to map and delineate the geology, structures relating to hydrothermal auriferous gold deposit.

1.3. Aims and Objectives

The main aim of this research is to enhance the exploration and discovery of gold mineralization using integration of ground magnetics and electrical (IP-Resistivity) geophysical methods related to tectonic or structural setting. The study seeks to integrate ground magnetic, electrical and structural datasets for better mapping of the hydrothermal related structures in the Sefwi belt. Based on quantitative and qualitative interpretation of the integrated geophysical methods, four main specific objectives are addressed in this research;

- map and predict the occurrence, geometry, direction and continuity of mineralization
- provide basis for the use of integrated geophysical studies
- map and delineate subsurface structural trends and the depth to magnetic sources of target areas.
- generate and update geological map of the project location

1.4. Justification

An Integrated geophysical and structural datasets has become an enhancing tool in structural mapping and therefore calls for such studies to be undertaken in the Sefwi belt. Within the past decades, until the early 2010, gold commodity has tremendously impacted positively on the global economy. Many exploration companies have flourished resulting in significant set up of mines and near-mine developments. The use of geophysical tools has proven to be a positive aid to these successful mines. Many authors have depended on one geophysical tool in their quest to define potential targets for gold mineralization.

In mineral exploration, as well as for environmental geology and hydrological studies the IP method has been used (Kiberu, 2002). Self-potential (SP) tool has excellent applications in geotechnical and engineering investigations, also in geothermal exploration (Corwin and Hoover 1979 and Anderson 1984) and in the search for sulphide ores (Corry, 1981, Yungul et al, 1950). Ramadan and Sultan (2004) used the magnetic technique for identifying massive sulfide zones. Additionally, integrated geophysical techniques were used for mineral exploration campaign (Macnae, 1979, and Smith, 2002).

In 2007, Golden Star Resources (GSR) embarked on ambitious geophysical studies on its Bogoso, Prestea and other concessions. These included Versatile TimeDomain Electromagnetic (“VTEM”), aero-magnetic and induced-polarization surveys which resulted in discovering “missing” target and helped in fully understanding the structural setting of the project area. This further aided in defining drilling targets in 2013.

In 2013, Castle Peak mining limited conducted Resistivity/IP- chargeability (Poledipole and gradient) geophysical survey on the Great Yorkshire and Canterbury prospects. This helped in delineating and ranking high-grade targets and discovery of the Akorade structure.

1.5. Scope of work and expected outcome

The project involves survey grid setup, magnetic and electrical (IP-Resistivity and Chargeability) data acquisition, processing, analysis and interpretation using Geographic Information System software (Geosoft, ArcGIS, MapInfo/Discover and Global mapper). The project seeks to delineate and constrain based on lithology, structural and geological trends related to complex hydrothermal sources through rigorous data inversions. The project is determined to address the following outcomes;

- Definitive potential gold mineralization
- Develop an inferred geometry and nature of mineralized body at depth
- Provides succinct drill targets for resource modeling and estimation

1.6. Structure of Thesis

The thesis is organized into six (6) chapters. Chapter one presents the background to the entire thesis, definition of the problem and the justification therein. The chapter additionally highlights the specific objectives related to the research, scope of work and structure of the thesis. Chapter two deals with literature review which focuses on the regional and local geological setting which deals with the major types of gold deposits found in Ghana and guidelines for the exploration of gold. This chapter also deals with description of the study area.

Chapter three addresses the theoretical background of the magnetic and electrical geophysical techniques used in the research. Chapter four outlines the materials and methods used in the survey setup. It also involves the data acquisition, processing and enhancement of anomalies for data interpretation. Chapter five presents the results obtained and discusses its interpretation from various maps acquired from the study. Finally, chapter six contains conclusions of the findings and suggests recommendations.



CHAPTER TWO

LITERATURE REVIEW

2.1 Regional geology and structural setting

Gold occurs as primary product in a wide generic of deposit types and settings around the globe. In the past decades, major progress has been seen that has resulted in the cataloging and insight into gold deposits. Exploration for gold is basically involved in defining of the footprints of gold deposits and integration of several definitive methods alongside geology for their efficient and effective identification and detection. Exploration techniques may involve geology, soil geochemistry, geophysics and structural signatures integrated in defining potential gold deposits. It is noteworthy; none of these methods are “stand-alone” in gold prospecting.

Numerous research findings have been made available on gold deposits in the last two decades that has led to the significant improvement in the meaning of models, the definitive deposit types or subtypes and the emergence of new nomenclature. Globally, thirteen types of Gold deposits that are significant are currently known, and each has its unique, well-defined features and environment of formation (Robert et al., 2007).

Robert (1997) and Poulsen (2000) proposed that most of these gold deposits can be categorized, that is, families of deposits that either formed by associated processes or that are unique products of large scale hydrothermal process. Hagemann and Brown (2000) classified main gold models as: (a) Orogenic, (b) Reduced Intrusive-Related (RIR) or (c) Oxidized Intrusive-Related (ORR).

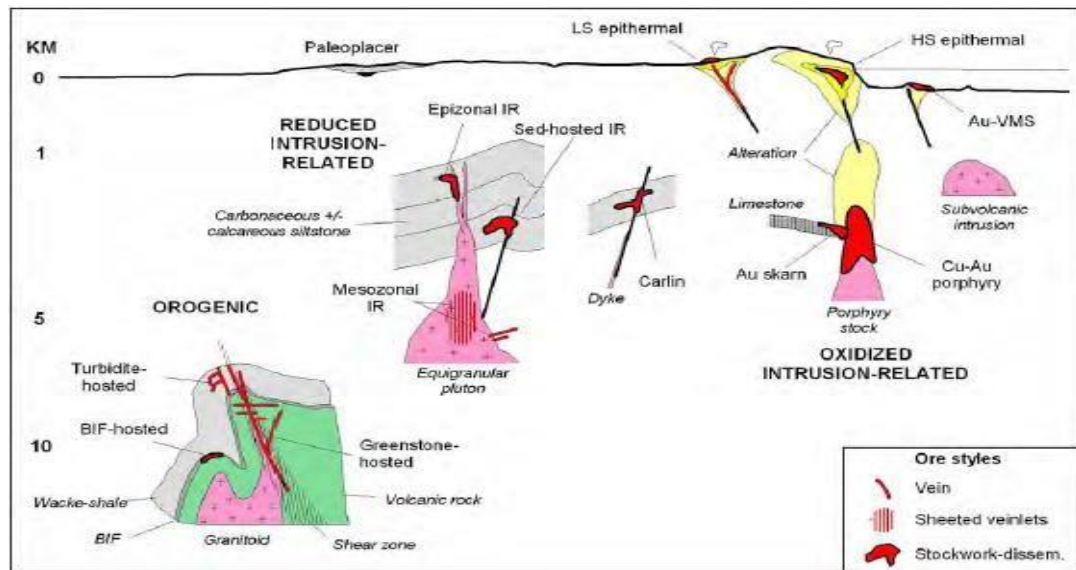


Figure 2.1 Gold systems and crustal depths of emplacement. Adapted from Poulsen, 2000 and Robert, 2004a.

The term orogenic was first reported by Groves et al. (1998). Originally, orogeny is applied strictly to syn-tectonic vein-type deposits formed at mid-crustal levels in transpressional settings (Robert et al., 2007). Principally, the Birimian/Eburnean units throughout West Africa can be associated with the orogenic type. However, the other two types aforementioned are also associated in some instances with the type a.

2.2. Types of gold occurrences

The BRGM group of France conducted a very extensive study of the ore deposits and tectonics of the Birimian orogenic belt of West Africa and developed a general classification scheme (Griffis et al 2002). The group description of the scheme is briefly set out below.

T1 Tourmalinized Turbidite hosted Gold deposits

T2 Disseminated Gold-Sulphides Deposits

T3 Tarkwaian Paleoplacers

T4 Mesothermal Auriferous Arsenopyrites and vein quartz mineralization

T5 Mesothermal Gold-Quartz vein deposits

Ghana contains six extensive and principal Birimian orogenic belt system associated with gold deposits. Regionally, gold occurrences conform to the Type 4 (Ashanti) and some also fit very well with the Type 5 (Griffis et al. 2002) whilst recent studies have proven the existence of Tarkwaian Paleoplacers within all the belts. However, gold deposits in Ghana can be broadly categorized into (i) vein systems (ii) Paleoplacers and (iii) alluvial, Griffis et al., 2002. The vein systems cover a very broad category and include a close association with disseminated sulphides.

2.2.1. Birimian-Hosted Deposits

This type of deposit is hosted by Birimian metasediments and metavolcanic and accounts for, from an economic viewpoint, about 75% of Ghana's gold production over the past 100 years, Griffis et al., 2002. Vein and stockwork systems with associated disseminated sulphides are important features of the Birimian-hosted deposits. Indeed, Paleoplacers of Tarkwa cannot be underestimated since they were the pacesetters of gold exploration by the early Europeans. Host rocks are usually argillites, greywackes, fine-grained sulphides, carbonates featuring extensive, steeply dipping vein systems (Griffis et al. 2002).

2.2.2. Intrusive Related Deposits

This type of deposit has not been previously observed as favourable host rocks though have been recognized in close association with typical vein-type occurrences as in Bibiani (Griffis et al. 2002). The mafic intrusive is pre-metamorphism but appears to post-date nearby belt granitoids and may be related to the extensive

mafic sills very common in the Tarkwaian sediments further north. Notable occurrences of intrusive related deposits related to gold mineralization are found in Bibiani, Ayanfuri, Obatan and Manso Nkwanta. Most of the mineralized stockwork in the Manso Nkwanta district have features similar to typical Ashanti-type deposits with free gold in the veins and vein selvages, which also contain fairly abundant pyrite and subordinate arsenopyrites although the latter does not appear to contain substantial gold. The alteration also features silica, carbonate, sericite and chlorite alteration in both the metasediments and granitoids.

2.2.3. Tarkwaian (Paleoplacers) Hosted Deposits

Over the past 100 years, the banket conglomerates of the Tarkwa district have produced over 10 million ounces of gold. The Tarkwaian hosted-deposit consists mainly of the banket conglomerates (Paleo-placers) and the vein quartz systems. Ghanaian professional trained in the UK, Thomas Sam, (1898) made the first publication on the geologic nature of the Tarkwaian Paleoplacers. Hirst, 1938 and Junner, 1943 established the general stratigraphy whereas Sestini (1973) did an extensive study on the sedimentology of the units. Of the two systems, the vein-type is mostly related to structural control. Other gold occurrences in Ghana can be categorized under Oxide and Laterites and late Quaternary alluvial (Griffis et al. 2002). More often than not, these occurrences are related to all the three main deposits aforementioned.

2.3. Gold belts of Ghana

Principal gold belts of Ghana are grouped with the greenstone/volcanic belts with which they are associated, (Fig. 2.2). In Ghana, productive gold-bearing belts are thought to be inclusive of an extensive geologic region. This region underlies Niger,

Mali, Guinea, Senegal, Liberia, Burkina Faso and Cote d'Ivoire. Throughout this West Craton Region, gold occurrences are along shear zones and found in some of the world's largest deposits. They also occur along shear zones that form the margins of belts or cut through them.

Belts are sandwiched between sedimentary rock basins which are protoliths of or partially derived from these volcanic belts. These sedimentary and volcanic rock units are classified as Birimian rocks and are aged between 2180 to 2130 million years approximately! Sedimentary rock assemblages are distinctive and are underlain by portions of quite a number of the Birimian belts. These sedimentary rock units may also include paleo-placer gravely units with inclusion of gold.

All sedimentary basins and Birimian belts along with Tarkwaian paleo-placers have actively been subjected to numerous tectonic events which have resulted in formation of faults, shears and complex folds which constitute known structural trends. All the six gold Belts are known to contain significant amount of gold, although few of the belts have seen enormous exploration and exploitation over the past decades. Contrasting the Ashanti and Sefwi Belts, the former has been world-famous gold producer over the past 100 years. The Sefwi Belt indicated in Figure 2.2 may be the next potential and prominent gold producer.

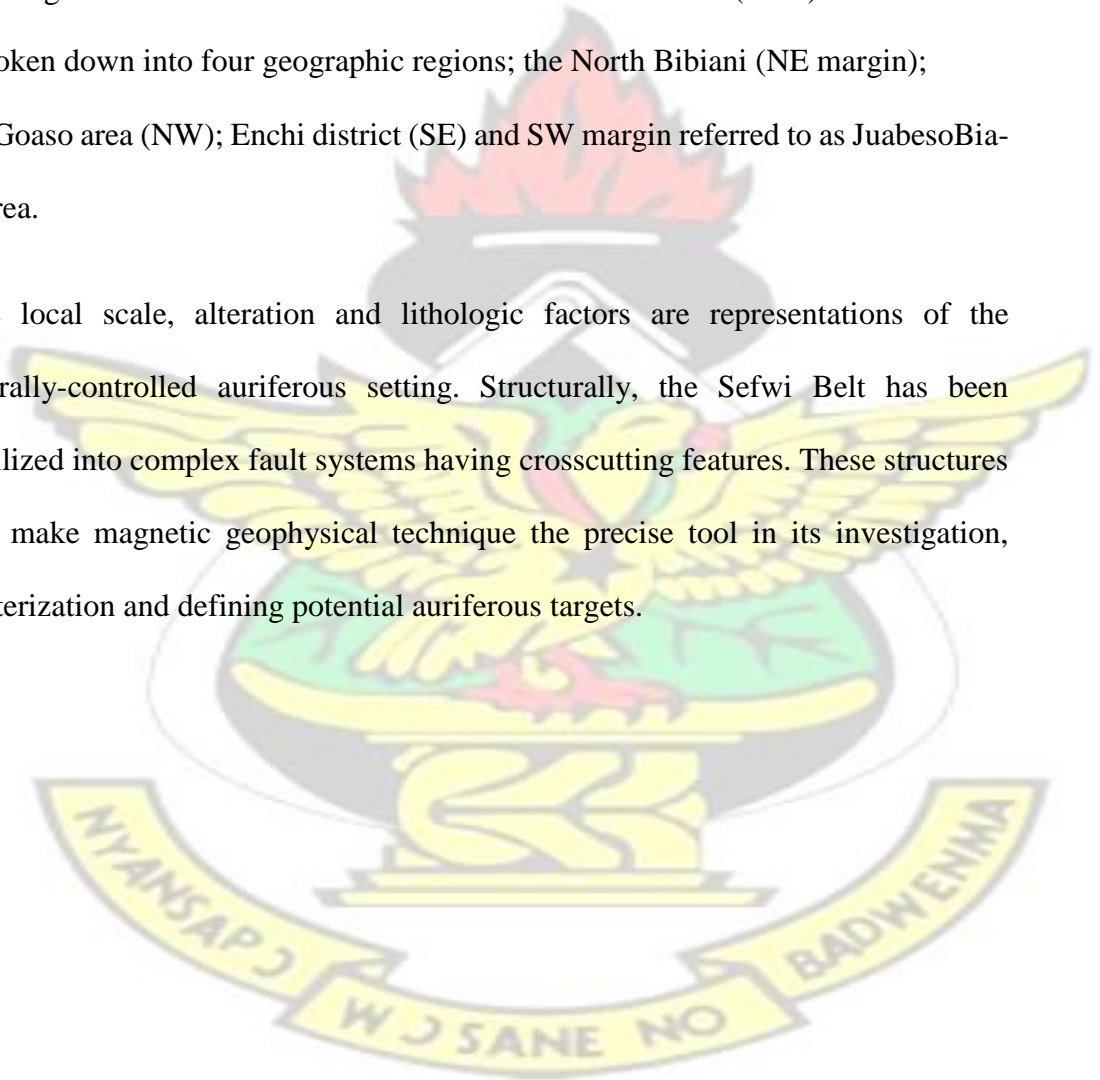
2.3.1. The Sefwi belt

The Sefwi Belt can be related to the main lode deposit of Ghana and notably one of the largest volcanic belts with prominent auriferous gold deposits on the south-east and north-west peripherals. Boyle (1979) noted that these types of lode deposits occur in

rocks of all ages (Archean to Cenozoic) and have broad similarities in relation to structure, mineralogy, alteration, geochemistry and regional setting.

The Sefwi belt, also known as Sefwi Bibiani Belt is a fairly typical Birimian volcanic belt of considerable width (40-60 km) and lateral extent (Griffis et al, 2002). It is predominantly of extensive belt-type diorite intrusive complexes, mafic volcanic and metasediments, some of these host considerable auriferous deposits as in Newmont's Mine along the north-western corridor of the belt. Griffis et al (2002) had the Sefwi belt broken down into four geographic regions; the North Bibiani (NE margin); North Goaso area (NW); Enchi district (SE) and SW margin referred to as JuabesoBia-west area.

At the local scale, alteration and lithologic factors are representations of the structurally-controlled auriferous setting. Structurally, the Sefwi Belt has been remobilized into complex fault systems having crosscutting features. These structures setting make magnetic geophysical technique the precise tool in its investigation, characterization and defining potential auriferous targets.



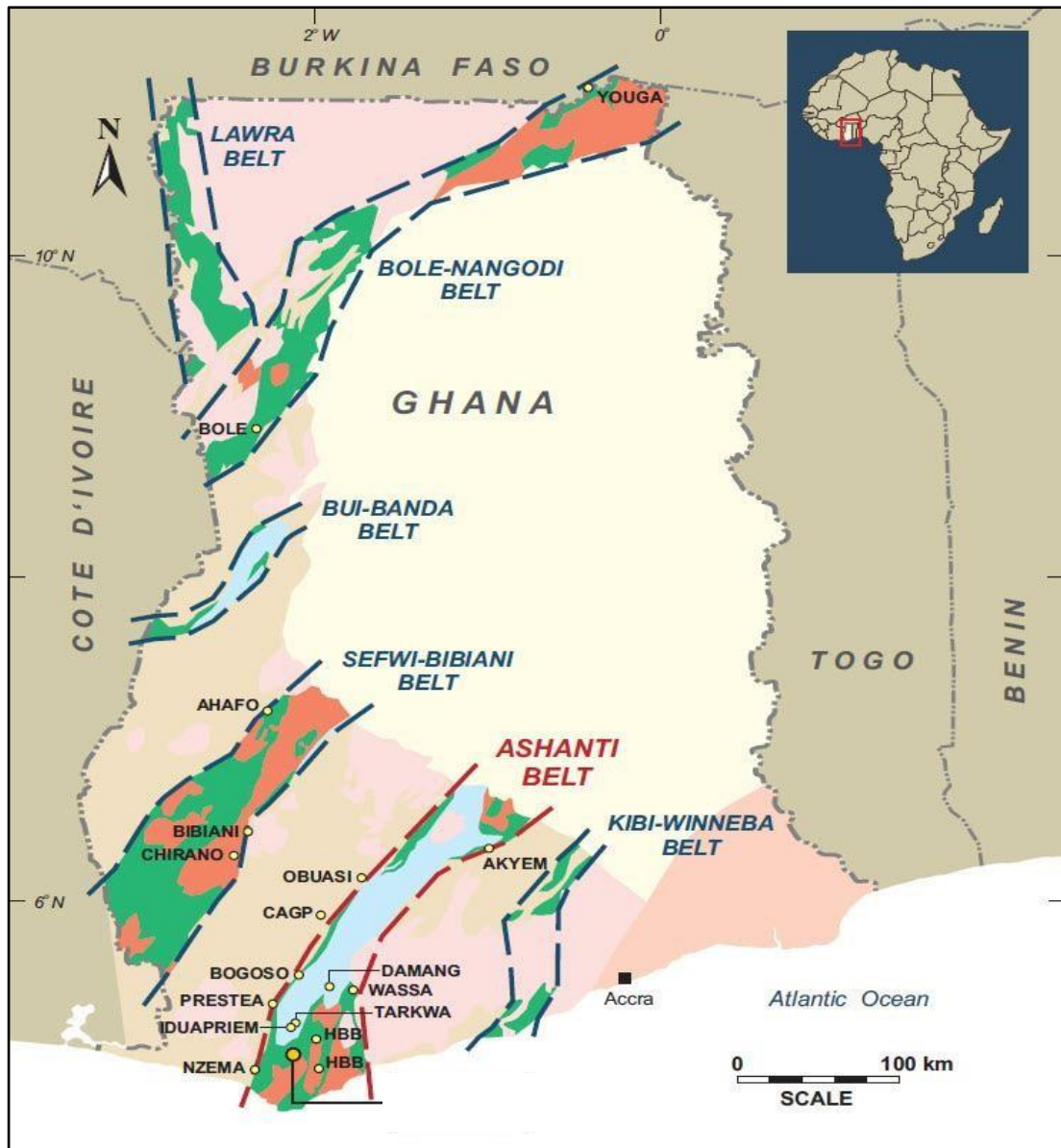


Figure 2. 2 Principal Gold belts of Ghana (Griffis et al, 2002)

In most areas, the Sefwi-Bibiani Belt is associated with strong silica-carbonate, albite-pyrite-sericite alterations. Other deposits types (e.g. Teekyere, south of Subenso) occur exclusively within folded metasediments that are strongly altered by chlorite, quartz, pyrite, carbonate, feldspar, sericite or combination of any of the four units.

2.4. Local Geology and Gold mineralization

The geology of the study area could be interpreted using regional aeromagnetic survey which is locally of very low resolution. However, thick weathering profile and concealed outcrops makes the use of ground base magnetic and electrical methods a necessity.

The study area is located 5 km North and 7 km South-West of Edukrom and Ankasi respectively. Regionally, the study area is within Birimian volcanic/volcaniclastic and Birimian sedimentary units and overlain by belt-type granitoid. The study area can be traced 100 km NE of known Kenyase mineralization configuration. The Kenyase-style mineralization is predominantly of meta-sediments to meta-volcanisedimentary units with varying weak to strong foliation trends. At the hanging wall of the Kenyase thrust zone overlays the belt granitoid. Hydrothermal alteration, notably sericite, quartz-carbonate and albite are widespread.

2.5. Project Area

The study area is within World Geodetic System (1984), Universal Transverse Mercator (UTM) 30 degrees North as in Table 2.1 and covers an area of 3.6 km² and a perimeter of 8.6 km.

Table 2.1 Study area boundary pillars

Pillar	UTM_East	UTM_North
P1	503020	695230
P2	502090	695860
P3	503830	698400
P4	504710	697830

The study area is located within Juabeso District of Western corridor of Southern Ghana as shown in Figure 2.3. The district capital Juaboso is located some 360 km to

the North of Takoradi, Western regional capital, and from Kumasi, the Ashanti regional capital a distance of 225 km. The Banda Ahenkro property straddle the projected south-westward extension of the Ahafo Shear Zone, which hosts Newmont's over 30 million ounce Ahafo Gold Mine.

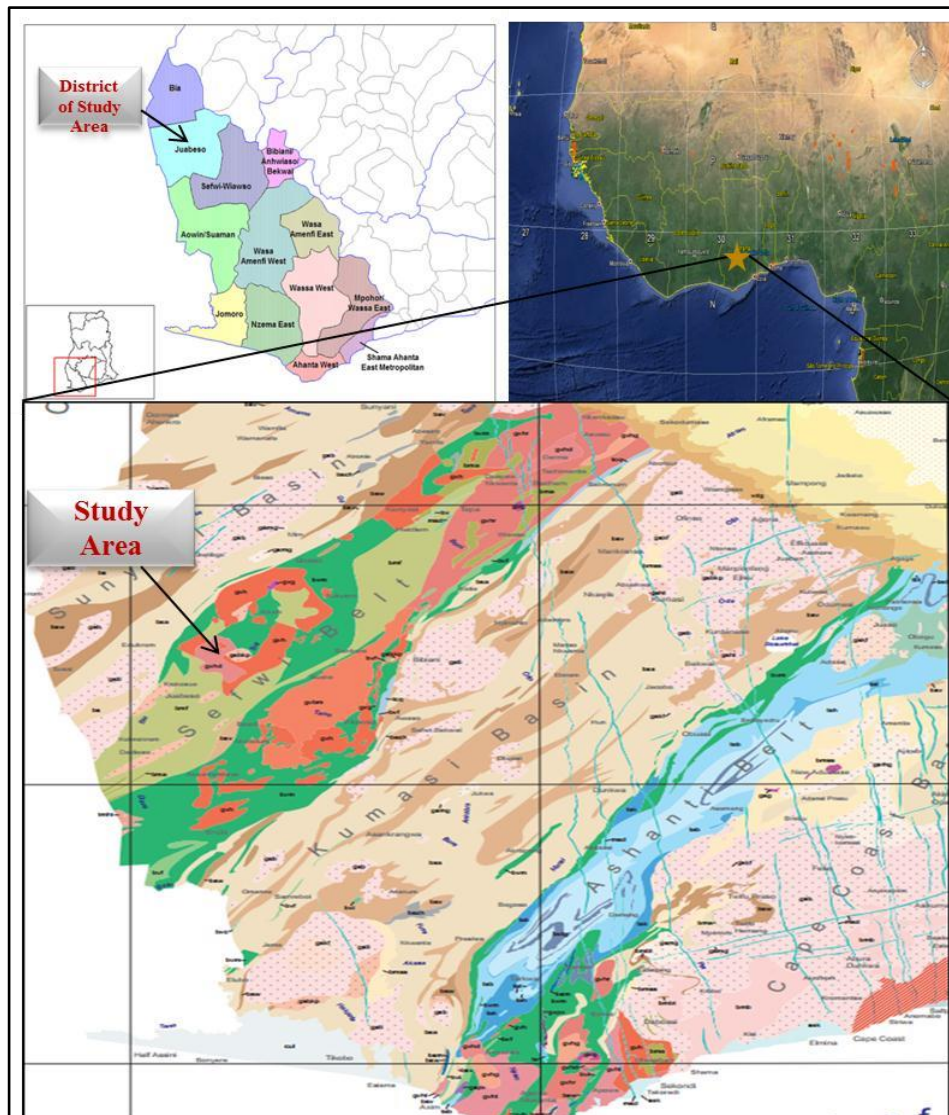


Figure 2. 2 Regional map, Google location map and geological map (Griffis et al, 2002)

2.6. Accessibility

The study area can be accessed by road through the Juabeso-Elubo to the village Kofikrom. From Kofikrom, a second class road heads southwest to Kwesi Adaekrom. A vast number of trails and tracks lead from Kwesikrom to Santasi which sits at the

north of the study area. A distance of 19 km would be covered from Juabeso to Kwesi Adaekrom through the second class road and about 3.5 km of trail to Santasi.

2.7. Climate and Vegetation

The study location is within the country's semi-equatorial climatic zones and have two peak rainfall patterns; September-October and between May-June respectively with annual mean rainfall figures between 1,250 mm and 2,000 mm (Ghanadistrict.com). Mean annual temperatures for the study area ranges between 25.5 °C and 26.5 °C. Relative Humidity also ranges from 75-90% during the wet season and 70-80% during the dry season. The relatively long periods of rainfall have been favourable for the nurturing of cash crops. However, there have been recorded cases of bush fires from the severe harmattan, which causes food losses and environmental risks.

The district's vegetation is of moist semi-deciduous forest type. Some of the important varieties include Esa, Edinam, Onyina, Odum, Wawa, Mahogany, Kyenkyen and Ofram. This may explain for the district being the hub of timber exploitation in the country (Ghanadistrict.com). The Juabeso district and the study area at large is known for the cultivation of cocoa, which is the heart of Ghana's gross domestic capital. The prominent food and cash crops grown are maize, plantain, vegetable, rice, cassava, oil palm, coffee etc.

2.8. Setting of Study Area

Juabeso district is among the rural districts of Ghana whose major economic commodity is agriculture. However, the agriculture is supported by minor activities such as trade and commerce, leather manufacturing, agro processing and banking. The district also earns foreign exchange from cash crops such as oil palm, coffee and cocoa,

and food crops such as cassava, rice, cocoyam, maize and plantain. Oranges, pineapple, coconut and pear are variety of fruits cultivated in the district.

KNUST



CHAPTER THREE

THEORETICAL BACKGROUND

3. Ground magnetic

3.1.1. Introduction

Magnetic surveying is a passive geophysical tool that exploits the contrast in the magnetic properties of rock-forming minerals. The aim of magnetic prospecting is to characterize the earth's sub-surface and to look for concentrations of anomalously high values of economic minerals. Magnetic surveying is thought to be the oldest of geophysical tools. However, it saw its full potential in the advent of airborne surveys after the Second World War (Reford and Sumner, 1964; Hanna, 1990).

The magnetic method has been utilized in mapping basement, locating faults, defining lithological contacts, archeological investigations, mapping salt domes and to better define targets through inversions. Magnetic survey has evolved from mapping basement (igneous) structures into new applications-oil and gas, geothermal resources, natural hazards and risk assessment, engineering structures, environmental studies and precious and base metal exploration. Magnetic surveys have had successes as an airborne tool, on ground and on sea. It has also been utilized for planetary studies as well.

3.1.2. Basic Concept

The earth possesses a permanent magnetic field as a result of its dynamo-thermal convection of its liquid iron outer core (Campbell, 1997). This force or flux extends into tens to thousands kilometers outer space, known as magnetosphere.

The magnetic flux of the earth can be likened to a magnetic flux within the vicinity of a bar magnet which flows from one end to the other. The S.I units of the earth's field intensity is expressed as nano-Tesla (nT) or Gamma (γ) where $1 \gamma = 10^{-3} \text{ T}$. The Earth's magnetic intensity is in the range of 25,000-70,000 nT, except for small levels of perturbations to the field intensity. The sought-after field precision is usually 1γ , or 10^{-5} of total field intensity of the earth. However, anomalies can result in few 100 γ amplitudes.

3.1.3. Magnetic Susceptibility

Rocks or rock forming minerals may have an inherent property to be magnetized in the presence of an applied magnetic field. This property of the rock forming mineral is its susceptibility. In other words, it is the degree to which a body placed in the earth's field is magnetized (Telford et al., 2004). This phenomenon is true for most rock forming minerals or rock units except for permanent magnets. That is, they may exhibit an induced magnetic field as a result of characteristic of the material when placed in the earth's magnetic field. Upon subjecting a magnetic material in a magnetic field, it experiences magnetization in the direction of the field. However, the magnetization is lost when the material is taken away from the inducing field. This observable effect is termed as magnetic polarization or magnetization.

For a material to behave as a magnetic, its inherent magnetic tendency is activated by the action of the magnetic field placed in it. Thus, this effect is known as magnetic polarization. The strength of the magnetizing force, H is proportional to the inducing field, J. Thus the induced magnetization, $J = kH$ where k is the material's magnetic susceptibility. With the exception of magnetite with $k=0.3$, most rock-forming minerals have much smaller susceptibility, usually of the order 10^{-6} .

Susceptibility, k depends on magnetic minerals characteristics in the rock, for a vacuum $\mu_r=1$ and $k=0$; where μ_r is the relative permeability (Keary et al, 2002). The susceptibility of a rock-forming mineral depends largely on composition, structure and percentage volume of magnetic minerals. It is also dependent on the state of magnetization and grain size. The relative permeability is related to absolute permeability, (μ) and permeability of vacuum (μ_0) by equation

$$\mu_r = \mu / \mu_0 \quad (3.1)$$

Table 3.1 Common Rocks with their magnetic susceptibility values (Telford et al., 2004)

MINERAL	SUSCEPTIBILITY
Quartz	-0.01
Rock Salt	-0.01
Calcite	-0.011
Sphalerite	0.4
Pyrite	0.05-5
Hematite	0.5-35
Illmenite	300-3500
Magnetite	1200-19200
ROCK	SUSCEPTIBILITY $\times 10^{-3}$ (SI)
Limestone	0-3
Sandstone	0-20
Shale	0.01-15
Schist	0.3-3
Gneiss	0.1-25
Slate	0-35
Granite	0-50
Gabbro	32874
Basalt	0.2-175
Peridotite	90-200

Susceptibility is dimensionless in the SI system; however negative susceptibilities exist for certain minerals and sedimentary rock units as shown in Table 3.1. The magnitude of susceptibility found in common rocks ranges over 2-3 orders. Highest susceptibilities are generally associated with basic igneous rock type, which explains its high constituent of magnetite. With increasing acidity of the rock constituent, the proportion of magnetite also decreases with a low susceptibility, k . An example is fresh

granite. Metamorphic rock unit has its susceptibility closely associated with the availability and abundance of oxides (O^2) at the time of its formation. Rocks of sedimentary origin on the other hand usually has a very low susceptibility and follows that structures related to sedimentary units rarely results in large magnetic anomalies.

Usually, an igneous body emplaced within sedimentary environment at near surface or deep seated, would give rise to a magnetic anomaly of high order of susceptibility. Notable causes of such magnetic anomalies include lava flows, dykes, folded, basic intrusions, metamorphic basement rocks, faulted sills. Among these and ore bodies that contain magnetite all generate magnetic anomalies of large-amplitude. The use of magnetics can be extended to the study of ancient monument of archeological interests. Examples include kilns and fire pits, jars, tombs etc. Magnetic anomalies can be used in the study of metamorphic thermal aureoles, to ascertain the thickness of sedimentary units and depth to basement rock units.

3.1.4. Rock magnetization

The magnetic field, whose amplitude is measured -as far as exploration geophysics is concerned- is the vector sum of;

- the field of the earth, defined from the onset as the dynamo action of earth's interior conductive fluids (Merril et al, 1996)
- induced field, which varies exponentially and originates outside the earth
- a field caused by magnetic remanence of the earth crustal materials (Doell and Cox, 1967) and,
- ionosphere (Telford et al, 1976) and cultural influences

3.1.5. Diamagnetism, Paramagnetism and Ferromagnetism

Generally, anomalies caused by magnetic influences are as a result of the inclusion of magnetic minerals such as marcasite or pyrrhotite that are contained in the rocks. Different kinds of magnetic materials exist based on quantum theory. According to quantum theory, two electrons can exist in the same electron shell as long as they spin in opposite direction (Kearey et al., 2002). This phenomenon allows all atoms to possess a magnetic moment. However, the magnetic moment of two such electrons, called paired electrons, cancel out. Rock forming materials can be divided based on their reaction to induced magnetic field placed on them.

3.1.5.1. Diamagnetism

Electron shells in diamagnetic materials are full meaning its electrons are all paired. Its magnetic effect is zero since the electrons spin contiguously in opposite direction. Diamagnetic minerals have negative k 's. Examples includes salt are quartzite.

3.1.5.2. Paramagnetism

In paramagnetic there is incomplete electron shells that results in a weakened magnetic field. A magnetic field when placed in an external field become induced.

Susceptibilities are positive. 20Ca - 28Ni element series falls within paramagnetic units.

3.1.5.3. Ferromagnetism

A special feature of paramagnetic minerals where groups of atoms align to form domains is termed ferromagnetic. Their magnetic susceptibilities values are larger than its paramagnetic elements. Nickel, Cobalt and Iron are the only three elements of ferromagnetic origin. Generally, there are three types of ferromagnetism; pure

ferromagnetism, ferrimagnetism and antiferromagnetic. Almost all magnetic materials that occur naturally belong to the ferrimagnetic unit. Examples include illmenite, magnetite and titanomagnetite. An example of antiferromagnetic minerals is hematite (Fe_2O_3).

3.1.6. The Curie temperature

Curie temperature is the temperature of demagnetization-loss of magnetism. At certain temperatures, most magnetic minerals may go through an abrupt change in their magnetic properties. Curie point when exceeded, the direction of magnetization reverses or disrupts accordingly. On the other hand, at certain lower temperatures, less than the Curie point, the magnetic minerals would keep their magnetization direction (Kearey et al., 2002). Examples include Fe 1382 °F, Ni 680 °F and Cobalt 2,050 °F. Magnetite forms the basis of major anomalies within the earth crust. To acquire information on the depth of causative bodies, knowledge of geothermal gradient and Curie temperature is paramount, which gives information of causative bodies at depth range.

3.1.7. Remanent Magnetism

A rock mass containing magnetic minerals will have an induced as well as remanent magnetization. Remanent magnetization in rocks is magnetization that would be present even when the inducing magnetic field is lost. It occurs in ferromagnetic materials and is due to an alignment of magnetic dipoles or magnetic domains at the atomic scale in the presence of an external field. When the inducing external magnetic field is changed, the material retains its own magnetism because of the ordering of the magnetic domains.

In many instances, rock forming minerals exhibit a permanent or Natural Remanent Magnetization (NRM) apart from the earth's inducing field of intensity, I , when the applied field, H is zero. The principal ones include chemical remnant magnetization (CRM), detrital remnant magnetization (DRM), isothermal remnant magnetism (IRM), thermoremanent magnetization (TRM) and viscous remnant magnetism (VRM).

Remanent magnetization can be explained easier using a hysteresis curve in Figure 3.1.

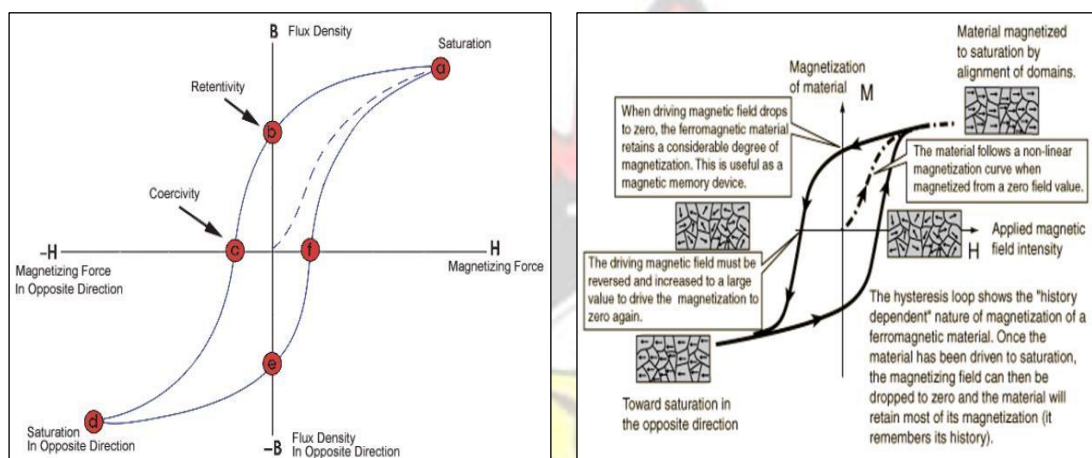


Figure 3.1 Hysteresis curve, Kearey et al., 2002.

3.1.8. Principle of Magnetic method

We can express the correlation between the flux density, B and the field strength, H in terms of k , a geologically diagnostic parameter. Note, permeability is related to flux density and the field strength by;

$$B = \mu.H \quad (3.2)$$

since $\mu = \mu_r \mu_0$ (from equation 3.1) where B denotes the flux density (measured in Weber/m²= Tesla) or the flux per unit area, also called the „magnetic induction“. B is a vector quantity.

then $B = \mu_r \mu_0 H$ rearranging and (3.3)

introducing $k = \mu_r - 1$

$$B = \mu_0 H + \mu_0 (\mu_r - 1) H = \mu_0 H + \mu_0 k H = \mu_0 H + \mu_0 J \text{ (since } J = kH \text{)}$$

Hence, $B = \mu_0 H (1 + k)$ (3.4)
and

$$J = kH \text{ (3.5)}$$

3.1.9. Magnetic anomalies

Telford et al., (1976) concluded that all shapes of magnetic anomalies are related to geomagnetic field and thus the directions are with respect to magnetic north (x direction), magnetic east, and so forth, the z-axis is positive downwards and we assume all locations are in the northern hemisphere.

Keary et al., (2002) used vector diagram to describe the normal geomagnetic field (Figure 3.2) and recognized that geomagnetic elements are related by B, H and Z which are respectively total field vector, horizontal and vector components, by;

$$B^2 = H^2 + Z^2 \text{ (3.6)}$$

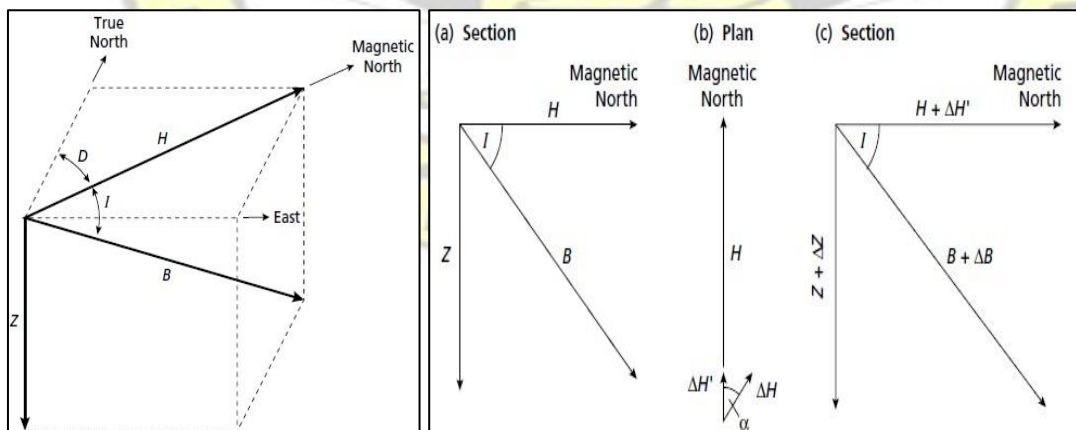


Figure 3.2 Geomagnetic elements, modified after Kearey et al (2002). Representation vector geomagnetic field modified after Keary (2002)

Assuming an anomaly is superimposed on the geomagnetic field, it causes a change ΔB in the strength of field vector, B . Similarly, H changes by ΔH , and Z by ΔZ so that equation (3.6) becomes

$$(B + \Delta B)^2 = (\Delta H + H)^2 + (\Delta Z + Z)^2 \quad (3.7)$$

If the anomaly produces a component in the vertical direction ΔZ and α at angle to the horizontal direction H . Where α is an angle to H (figure 3.2b) it is only that part of ΔH in the direction of H given as $\Delta H'$ that would contribute to the anomaly, (Keary et al., 2002). Therefore equation (3.7) then becomes

$$(B + \Delta B)^2 = (H + \Delta H')^2 + (\Delta Z + Z)^2 \quad (3.8) \text{ However, } \Delta H' \text{ is given by}$$

$$\Delta H' = \Delta H \cdot \cos \alpha \quad (3.9)$$

Expanding equation (3.9), equation (3.7) substituted and neglecting insignificant terms in Δ^2 , equation (3.9) reduces to

$$\Delta B = \Delta H' \frac{H}{B} + \Delta Z \frac{Z}{B} \quad (3.10)$$

Substituting equation (3.10) and inserting angular descriptions of geomagnetic element ratios ($Z/B = \sin I$ and $H/B = \cos I$, from figure 3.2, section (a)) where I is the inclination angle of the geomagnetic field,

$$\Delta B = \Delta H \cos I \cos \alpha + \Delta Z \sin I \quad (3.11)$$

Kearey et al (2002) demonstrated an anomalous small isolated magnetic pole of strength m , can be calculated from this approach. That is at the observation point, the

effect of this pole is a unit positive point which is situated at a radial distance from the observation point, at a horizontal distance x , and at a depth z (Figure 3.3).

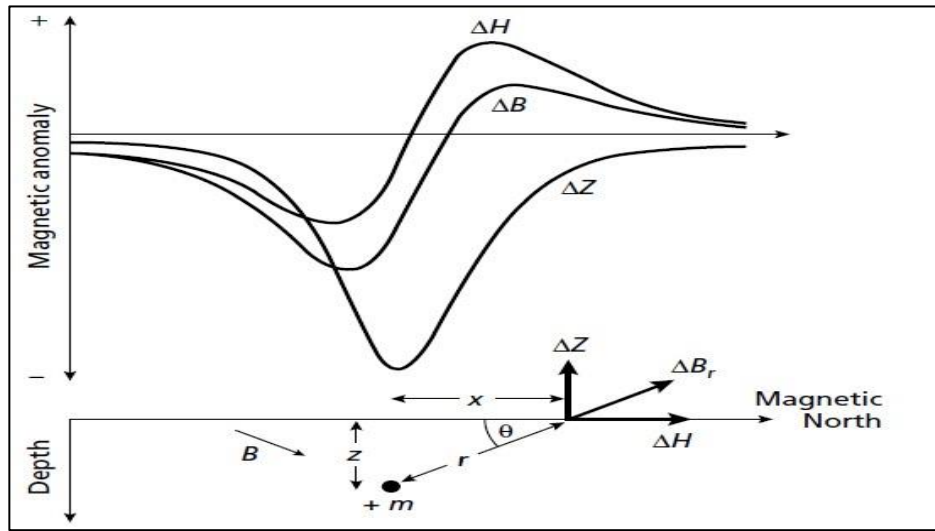


Figure 3.3 The horizontal (ΔH), vertical (ΔZ) and total field (ΔB) anomalies due to an isolated positive pole modified after Kearey et al (2002).

The field produced by this anomaly is given as;

$$\Delta B = \frac{C_m}{r^2} \quad (3.12)$$

where;

$$C = \frac{\mu_0}{4\pi} \quad (3.13)$$

the horizontal (ΔH) and vertical (ΔZ) force components can be calculated by resolving in the related directions;

$$\Delta H = \frac{C_m}{r^2} \cos \theta = \frac{C_m x}{r^3} \quad (3.14)$$

$$\Delta Z = -\frac{C_m}{r^2} \sin \theta = -\frac{C_m z}{r^3} \quad (3.15)$$

3.1.10. Magnetic survey instruments

Magnetic surveys are carried out with magnetometers, which measure the total magnetic field with high precision. Because the earth's magnetic field varies slightly from day to night, and with solar activity, it is important to use a base station magnetometer to record the daily or diurnal changes in the magnetic field at a fixed point. The base station should be established in an area with low spatial magnetic variation. The base station values can be used to correct all the rover readings.

3.1.10.1. Magnetic balance

Magnetic balances were useful before and during the WWII, which were generally mechanical instruments (Telford et al., 1990).

They were however, replaced by the flux-gate magnetometers which made the magnetic balance outdated! The magnetic balance has enabled the existence of huge data sets, available today. One of the known magnetic balance is the Schmidt magnetic balance. The magnetic balance is a relative instrument due to a simple reason that its magnet pivots about a point that is different from the center of gravity. At the center of gravity, the gravity effect balances with the torque of the magnetic field of the earth. The magnetic field which is a function of the angle of pivot is measured by a light beam that is projected onto a scale.

3.1.10.2. Flux-gate magnetometer

During the WWII the flux-gate instrument was basically developed in the use of detecting submarines in warfare (Telford et al., 1990). It has found its usage predominantly in aeromagnetic survey due to its continuous measurements. Its construction requires two coils wound in opposition and current is passed through to induced magnetization. An inducing magnetization is measured by the two secondary

winding and these two cancel out in the absence of the Earth's field. The opposing coils are subjected to an alternating current in the absence of the Earth's field, to saturate them. The Earth's thereby serves two purposes; it opposes one and reinforces the other. The secondary coils get out of step after the induction of the voltage. The result is a series of pips whose height is proportional to the ambient field.

3.1.10.3. Proton precession magnetometer

Nuclear magnetic resonance gave birth to the proton precession instruments. Protons, like most atomic nuclei, possess magnetic moment that causes it to precess around its ambient magnetic field. The PPM has container of oil or water which acts as its source of protons. A coil is wound around the oil/water container. A field of about 50-100 oersteds are produced when a current is applied across its ends. The container is not oriented such a way to align the field parallel to the Earth's magnetic field. The frequency of the precession is measured when the current is abruptly removed. This is when the protons realign themselves to the Earth's field.

The protons take about 3 seconds to align fully when the alternating current is applied. This effect mimics an exponential relationship. However, it takes significant time for the buildup of the precession after the removal of the applied field intensity or the ambient field. An accuracy of 1 cycle in 50,000 (1 Gamma) is expected to measure about fifty thousand cycles which takes about ½ seconds and a strength of about ten micro volts. Most PPM's have a precision of about 1 Gamma but other available models could record precisions as good as 0.01 γ or 0.1 Gamma. Other magnetometers includes the overhauser effect proton magnetometer, alkali vapour, magnetic gradiometer and the squid system.

3.1.11. Magnetic Survey Design and data acquisition

Magnetic survey design and data acquisition involves the setup of the profiles lines and subsequent sampling of magnetic measurements. The survey is performed perpendicular to the general strike of the perceived body so as to aid in the modeling of the anomaly.

As a quality control measure for detecting magnetic storms and diurnal drifts, the base stations are periodically tied-in at about two to three hourly intervals. However, a continually-reading base station or automatic magnetometer can be used when necessary. The operator must:

- Replicate readings for precision checks
- Set up base station and avoid metallic objects that cause interference

3.1.12. Data Reduction and Processing

Data processing involves all operations applied to the data from the acquisition to the interpretation stage which may be done through maps, digital data sets, contours or profiles. This stage also takes into account the meticulous steps in damping spurious noise and signals that come along with the crustal anomaly, thereby increasing noise-to-signal ratio. Data reduction and processing also involves the elimination of effects of time-varying external fields such as IGRF and diurnal effects.

3.1.13. Data presentation and enhancement

There are several ways to present data for post processing and interpretation. The corrected data –conveniently called diurnal-corrected- can be presented or visualized in the form of contour maps, images and stacked profiles (Milligan et al, 1997) or bipolar plots (Gyngell, 1997). In profiles and 3D maps, magnetic anomalies are

indicated by peaks, and in the case of the contour maps, close and high contour values indicate magnetic minerals (Keary et al., 2002).

3.1.14. Magnetic data filtering

Magnetic data filtering is a prelude to magnetic data interpretation and involves a wide range of transformations of the processed data that assist in its ultimate interpretation. These usually involve the application of mathematical filters or models. The objective is to make anomalies simplified, define prominent interests and make them pronounced and others less significant and finally relate the measured field anomalies to rock properties. Common filtering tools include reduction to pole (RTP), regional-residual separation, upward-downward continuation, derivative-based filters.

3.1.15. Qualitative interpretation

Qualitative interpretation of magnetic map, which is one of the initial stages of interpretation, involves the recognition of diagnostic shapes, trends of anomalies that can be related to geologic structures or rock units (Kearey et al., 2002). The shape, quantity and distribution of its magnetic minerals control the strength of a rock's magnetization. However, this constitutes a very small proportion of the bulk rock medium. Qualitative interpretation of magnetic anomaly basically involves visualization-based contour maps. Such interpreted maps may be related to lithology, alterations, folds, lineaments, faults, dikes etc.

3.1.16. Quantitative interpretation

Quantitative interpretation of magnetic anomaly attempts to give a reliable estimate of the direction, size, shape and depth of magnetic sources. It is complementary to qualitative interpretation. This technique is broadly characterized as curve matching,

forward or inverse modeling (Telford et al., 1990). In 1982, Thompson developed a technique known as Euler deconvolution method, to process magnetic data and to convolve them to a point source at depth. Equation 3.16 is known as Euler deconvolution equation. For an arbitrary specific structural index the depth and location for various targets can be resolved from these first order derivatives (x,y and z).

$$(x - x_o) \frac{dT}{dx} + (y - y_o) \frac{dT}{dy} + (z - z_o) \frac{dT}{dz} = N(B - T) \quad (3.16)$$

where; (x_o, y_o, z_o) is the source of magnetic anomaly, (x, y, z) is the total magnetic field detection points B is the regional magnetic field. N is the fall-off rate magnetic field measurement else known as the structural index (SI).

3.2. Electrical method

3.2.1. Introduction

In general sense, geophysical electrical prospecting may be defined as prospecting for minerals by employing electrical current (direct or low-frequency alternating current) for delineating mineral deposit and geological structures. Electrical methods depend on the differences in the electrical conductivity (or resistivity) of different rock types or minerals. So it follows that the physical properties measureable is the electrical resistivity or conductivity. Many rock-forming minerals are bad conductors whereas certain minerals like pyrite, chalcopyrite are very good conductors. The range of resistivity has large values compared to other physical quantities that are mapped with most geophysical tools. Additionally, soils and rocks in a prospecting location can vary in magnitude in several orders. Resistivity of some rock types, rock-forming minerals and chemicals are presented in table 3.2.

Table 3.2 Resistivities of rocks, minerals and chemicals adapted after Lowrie (1990)

Material	Resistivity ($\Omega \cdot m$)	Conductivity (Siemen/m)
Igneous and Metamorphic Rocks		
Granite	$5 \times 10^3 - 10^6$	$10^{-6} - 2 \times 10^{-4}$
Basalt	$10^3 - 10^6$	$10^{-6} - 10^{-3}$
Slate	$6 \times 10^2 - 4 \times 10^7$	$2.5 \times 10^{-8} - 1.7 \times 10^{-3}$
Marble	$10^2 - 2.5 \times 10^8$	$4 \times 10^{-9} - 10^{-2}$
Quartzite	$10^2 - 2 \times 10^8$	$5 \times 10^{-9} - 10^{-2}$
Sedimentary Rocks		
Sandstone	$8 - 4 \times 10^3$	$2.5 \times 10^{-4} - 0.125$
Shale	$20 - 2 \times 10^3$	$5 \times 10^{-4} - 0.05$
Limestone	$50 - 4 \times 10^2$	$2.5 \times 10^{-3} - 0.02$
Soils and waters		
Clay	1 - 100	0.01 - 1
Alluvium	10 - 800	$1.25 \times 10^{-3} - 0.1$
Groundwater (fresh)	10 - 100	0.01 - 0.1
Sea water	0.2	5
Chemicals		
Iron	9.074×10^{-8}	1.102×10^7
0.01 M Potassium chloride	0.708	1.413
0.01 M Sodium chloride	0.843	1.185
0.01 M acetic acid	6.13	0.163
Xylene	6.998×10^{16}	1.429×10^{-17}

3.2.2. Conduction in rocks

The conduction of electric current in a medium is basically a molecular property.

Generally there are three ways of electric conduction;

- Electronic (metallic) conduction: this is due to electron mobility and an examples are sulphides
- Electrolytic (ionic) conduction: takes place in the electrolysis of solutions due to transport of ions. This type is also known as electrochemical and is governed by Achie's (1942) Law.
- Dielectric conduction: This type possesses virtually no electrons or ions to provide conduction. Conduction only occurs on the surface of these materials.

3.2.3. Electrical resistivity

For any given material the electrical resistivity is a function of various geological parameters such as the degree of saturation in the pore spaces. It is also closely linked

to the mineral grains as well as the contents of the fluid contained in the matrix. Some specific electrical resistivity ranges can be related to certain materials, however, generally, the electrical resistivity of most materials are not diagnostic. Apparent resistivity is calculated from measured potential between two or more electrodes and known current injected into the ground between two electrodes. For many decades the electrical resistivity surveys have seen its successes in the geotechnical, mining and hydrogeological investigations. It has also been utilized in environmental surveys recently.

3.2.3.1. Basic concept electrical method

Resistivity (ρ) which is an inherent physical property of a substance is its ability to resist the stream of current by a unit cube of that substance when voltage is applied across the opposite faces. The resistance (R) offered by the substance with regular shapes such as cylinders, parallelograms and cubes can be determined with the formula,

$$\rho = RA/L \quad (3.17)$$

where ρ is the resistivity of the substance, L , length, and cross-sectional area, A of the substance.

If A is in metre-squared, L in meter, R is in Ohms, then $\rho = \text{Ohm-metre}$

The inverse of resistivity is termed as the conductivity (σ) and the inverse of resistance is conductance. Resistivity has the SI unit Ohm-meter and whereas its reciprocal is conductivity, that is Siemens per meter. It follows that $1 \text{ Ohm}^{-1}\text{m}^{-1}$

$$= 1 \text{ Sm}^{-1}$$

3.2.3.2. Current flow in the ground

If we consider figure 3.4 as representing the earth of a fictitious and electrically homogenous semi-infinite medium, with a single electrode point (Keary et al., 2002). In figure 3.4b, a potential drop ($-\delta V$) is caused between two ends of the element when a current, I is passed through a cylinder. According to Ohm's Law; the resistance, the current and the potential difference are related by

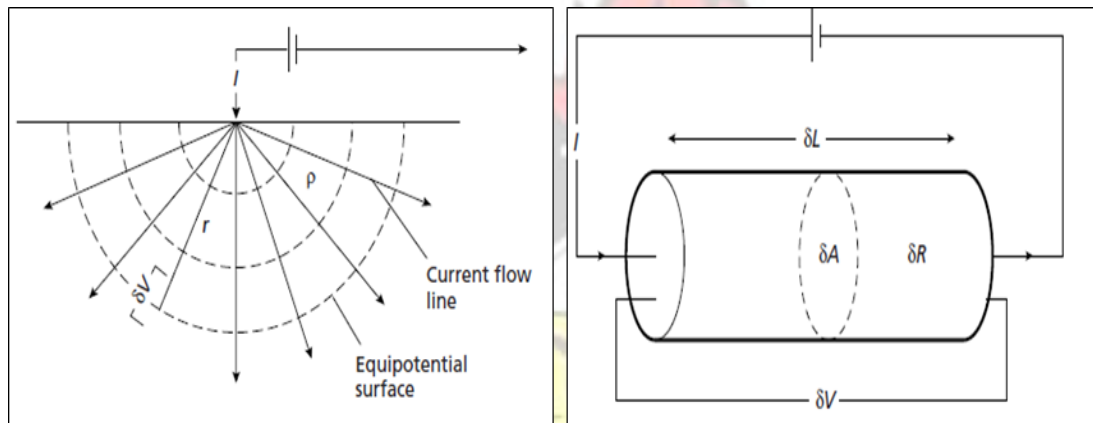


Figure 3.4 (a) Current flow from a single surface electrode (b) parameters used in defining resistivity

$$-\delta V = \delta R I, \quad (3.18)$$

hence, from equation (3.17) and substituting;

$$\frac{\delta V}{\delta R} = -\frac{\rho I}{\delta A} = -\rho i \quad (3.19)$$

Where $\delta V/\delta R$ represents the potential gradient in voltm^{-1} and i the current density in Am^{-2} . The shell has a surface area of $2\pi r^2$ and at r distance from the electrode, the current i is given by

$$i = \frac{1}{2\pi r^2} \quad (3.20)$$

Hence, from equation (3.19), the potential gradient can be associated with the current density by

$$\frac{\delta V}{\delta r} = -\rho i = -\frac{1}{2\pi r^2} \quad (3.21)$$

Obtaining the potential V_r at a distance, r by integrating

$$V_r = \int \delta V = \int \frac{\rho I \delta r}{2\pi r^2} = \frac{\rho I}{2\pi r} \quad (3.22)$$

Consider current I and $-I$ at electrodes A and B respectively where A and B are pair of electrodes. The current source at A and the sink at B is the arithmetic sum of the potential contributions of V_A and give as $V_C = V_A + V_B$. The apparent resistivity can be derived from equation (3.22) by;

$$\rho_a = \frac{2\pi \Delta V}{I \left\{ \left(\frac{1}{r_A} - \frac{1}{r_B} \right) - \left(\frac{1}{R_A} - \frac{1}{R_B} \right) \right\}} \quad (3.23)$$

The apparent resistivity of a geological formation is equal to the resistivity of fictitious homogeneous and isotropic medium in which for a given electrode arrangement and current strength the potential difference measured is equal to that of a given homogeneous medium. The apparent resistivity depends upon the geometry and resistivity of the elements constituting the given medium. The apparent resistivity is not the sub-surface's physical property but the true resistivity. To obtain the real physical or true resistivity values of a medium, all field resistivity measurements are subjected to interpretation techniques or inversions.

Equation (3.23) can be re-written with the introduction of depth of penetration or depth of investigation, K by;

$$\rho = 2\pi K \frac{V}{I} \quad (3.2)$$

3.2.3.3. Survey design and data acquisition

Resistivity measurements rely on the type of configuration or array type, which is related to the electrode spread and the geometric factor, K . Stakes of steel with bronze jackets, copper and other less desirable steel are used as current electrodes which are usually 50 cm length. In engineering applications, typical instruments used as current sources range from 2 mA through 500 mA.

To eliminate telluric current and electrode polarization effects special provisions must be complied due to the use of direct current. An unglazed ceramic pot usually in the form of porous pot is designed to be used as a non-polarizing electrode, which usually contained in them a metallic electrode that is copper in saturated copper sulphate solution.

Telluric currents are naturally occurring electric fields which may be neutralized by applying a technique known as bias potential. Bias potential tends to balance or tends to negate the effect of the potential electrodes before energizing the direct current electrodes. Other techniques to use are adjusting the bias potential frequently or using polarity-reversal switch. Layout should be done with non-conducting instruments or to look out for rails, pipes, metallic fences or other tools that may cause short-circuiting. Again, other electrical noise may exist; power lines, cables may interfere with the data acquisition. Recently, modern resistivity instruments have the capability for data averaging or stacking.

However, there are two techniques in the data acquisition, namely the Vertical Electrical Sounding, VES (resistivity sounding) and Horizontal Electrical Profiling, HEP (resistivity profiling). The common array types employed are the Werner and Schlumberger. These array types or configuration may have its unique sensitivities as

well as their merits and demerits. The scope of work, the ground conditions and even labour requirement to accomplish a particular task would affect the choice of array. Other crucial recommendations to meet are the understanding of the sensitivity to dipping interfaces (Broadbent and Habberjam 1971) and lateral inhomogeneities (Habberjam and Watkins 1967a; Barker 1981).

3.2.4. Induced Polarization

Induced Polarization (IP) may be is an addition to the electrical resistivity technique which utilizes rocks or rock-forming minerals' ability to store electrical charges. Kearey et al., (2002), indicated that the phenomenon of IP was to have been noted by Conrad Schlumberger as early as 1912.

The Second World War accelerated its use as potential military applications were identified. The use of IP in subsurface exploration thrived so well during period of 1960's through 1970's and also accompanied by improvement in sensitivity of instruments, deeper knowledge of IP theory and new methods of data interpretation. Today, it has become one of the most recognized techniques in mineral prospecting, particularly for investigating disseminated metallic ores. One reason is that the resistivity and EM methods do not give adequate information for their location and may, sometimes fail. Secondly, recent developments in instrumentation have indeed helped in carrying out the resistivity and IP measurements in the field simultaneously. Thirdly, any of the electrode configurations used in the field in ordinary resistivity work can be employed for IP measurements as well.

3.2.4.1. Basic concept on induced polarization

When a direct current is introduced into the subsurface by the use of dual current electrodes, a voltage is seen across its measurable two potential electrodes. When the current is interrupted suddenly, the potential voltage does not reduce to zero.

However, it would decay slightly after an initial decrease from its original steady-state value and takes many seconds to drop to zero (Figure 3.5). The direct current is switched off or dropped at a certain time t_0 . Subsequently, there is now initial large drop from the steady-state value ΔV_c , where the measured potential difference decays finally to zero. The sequence is further repeated when the current is switched on at t_3 . The time increment t_1-t_2 is represented by a shaded area under the decay curve in figure 3.5.

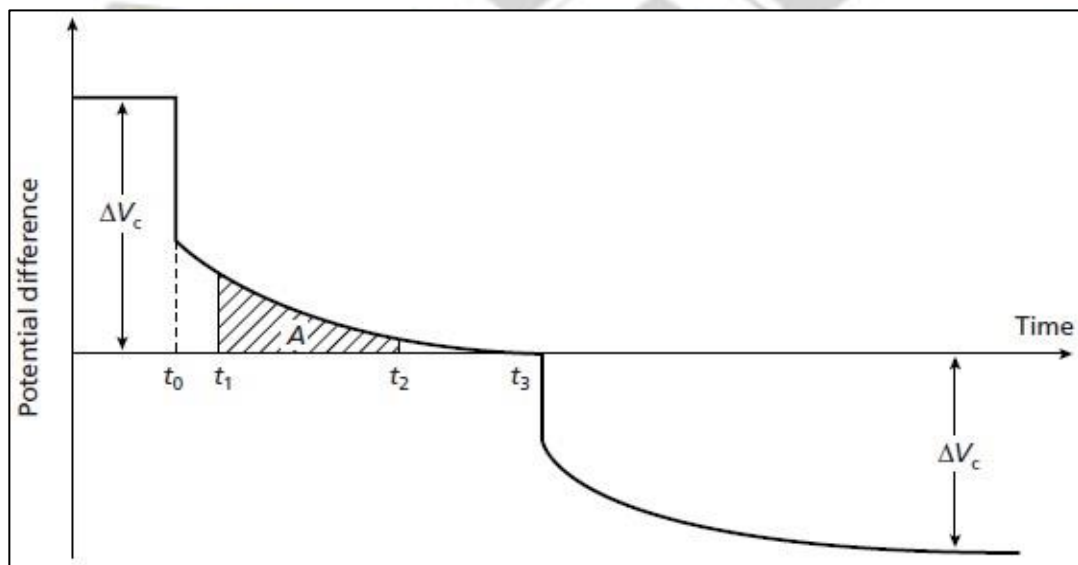


Figure 3.5 The phenomenon of IP, adapted from Kearey et al., (2002).

In general, this decay time may be in the order of a few seconds or sometime even minutes. When the current comes on again, there is an abrupt initial increase in the potential. However, the potential further builds up over the same time interval to the

original maximum amplitude. This is called IP Phenomenon. The complexity of rocks and soils conductivity response is basically dependent upon the surface chemistry, micro structure and bulk fluid composition.

The exact causes of IP effect may be reasonably understood under two main mechanisms-membrane and electrode polarization (Figure 3.6).

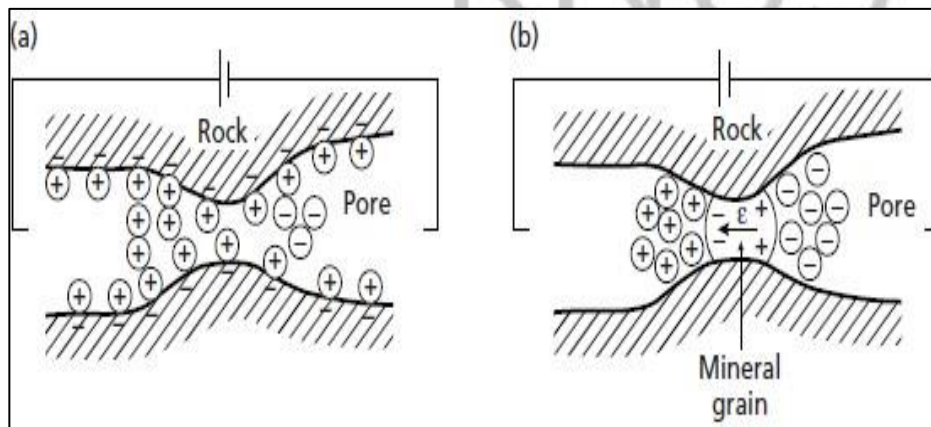


Figure 3.6. IP mechanism: (a) surface polarization and (b) over-voltage polarization.

Telford et al., (1990) indicated that this electrochemical energy storage is as a result of (a) effective porosity of the structure of the rock and (b) interaction between electronic and ionic conductivity where metallic minerals are present.

- Membrane polarization: This phenomenon is more pronounced in clays. There usually exists a net negative charge at pore fluids-rock minerals interface. Positive cloud is produced within the pore space when positive ions are attracted to them. Additionally, positive charges are able to migrate when an electric field is induced within this cloud but negative charges are blocked. When the electric field is removed, the imbalance in ionic concentration diffuses back to normal producing a measurable IP response.

- Electrode (overvoltage) Polarization: This is basically caused by the presence of metallic minerals. When this electronically conducting metallic mineral blocks the flow channel, charges build up when electric field is applied. This opposes the current flow and the metallic mineral becomes polarized. The ions, however, diffuses back upon removal of the induced electric field. This effect results in or gives a measurable IP effect.

3.2.4.2. Survey Design and measurements

Survey setup and design is similar to resistivity measurement and basically data acquisition is done simultaneously. However, depending on instrumentation the transmitter and receiver may either be standalone equipment or consolidated into one complete console. Induced polarization is very elaborate and bulky and uses ten times current to that of resistivity setup. In practice, Schlumberger, pole-dipole and double-dipole are the most effective.

However, any standard electrode array may be employed in theoretical sense. Telluric currents cause similar anomalous effects to those encountered in resistivity measurements. IP measurement can be carried in two different modes- Time and frequency domains.

- Time Domain: Induced polarization is said to be in time domain when the measurements or sampling involves monitoring decaying voltage after a drop in current. Chargeability is the measured parameter and is defined as the area A beneath the decay curve. This curve is basically over a certain time interval (t_1-t_2) and normalized by the steady-state potential difference ΔV_C (Fig. 3.5). Shortly after the cut off of the polarizing current, and at a specific time interval, the Chargeability M , (eq. 3.33) is measured.

$$M = \frac{A}{\Delta V_C} = \frac{1}{\Delta V_C} \int_{t_1}^{t_2} v(t) dt \quad (3.33)$$

- Frequency Domain: When IP effect is a measure of apparent resistivity at two or more AC frequencies, the phenomenon is termed Frequency-domain technique. The IP-effect is measured as a percentage of frequency effect (PFE) and is given by:

$$PFE = \frac{\rho_{low} - \rho_{high}}{\rho_{low}} \times 100 \quad (3.34)$$

Another measure, known as the Metal Factor is intended to correct for the resistivity of the host rock and the surrounding electrolyte. The unit of measurement of metal factor is mhos per meter (Siemen per meter) and is given by

$$\text{Metal Factor} = \frac{PFE}{\rho_{low}} \times 2\pi 10^5 \quad (3.35)$$

3.2.5. Processing of Resistivity and IP Data

Induced polarization and resistivity data are generated and recorded automatically and simultaneously by the resistivity console. The data is uploaded into appropriate format and processed using inversion software. Normalizing resistivity and chargeability measurements concurrently is the most crucial step in data processing.

Basically, IP measurements are presented as a pseudo-section in which readings are plotted so as to reflect the depth of penetration. Values are manually plotted to reflect the increasing penetration depth as the dipole separation distance increases. The values may be contoured as well. Vertical electrical sounding resistivity data can also be presented in the same manner with the plotted electrode separation proportional to the depth of investigation. Pseudosections give only a crude representation of the IP response distribution at depth. For example, the measure of the true dip of an

anomalous body is far from the apparent dip measured from the IP set up. The final step in electrical resistivity-IP data processing is to iteratively model and invert for the true chargeability-resistivity values of the subsurface. The result of the inversion is to find a two dimensional (2D) estimate of chargeability and resistivity structure that provides theoretical data closely matching measured data.

CHAPTER FOUR

METHODOLOGY FOR DATA ANALYSIS

This chapter focuses on the materials and methods that were used in the execution of exploration program. The main equipment used for the ground magnetic survey is the Geometrics 859 magnetometer. In the Resistivity and Induced polarization surveys the main instruments used were the high-powered voltage transmitter (VIP 4000) manufactured by IRIS Instruments (France), its Elrec pro receiver, porous pots, and electric cables. Planning and execution of a successful geophysical survey depends on the choice and sensitivity of equipment. This involves the knowledge of the site, scope of work, size and trend of anomaly, time, budget and environmental constraints.

The methods used in the research include data collection, quality control and data validation, data processing, data enhancement and interpretation. Each of these processes is outlined below, and has contributed significantly to the interpretation of the data.

4.1. Data Processing software

The data processing and modeling software used in the data manipulating and enhancement for interpretation are herein listed below

- Oasis Montaj (2008)
- RES2DINVx32 ver. 3.71
- Global Mapper 11
- MapInfo 10.5 and Discover 11.0

The different steps in capturing spatial data, extraction of spatial features and integrating spatial features to generate a predictive model by the above methods are summarized in the flow chart (Figure 4.1).

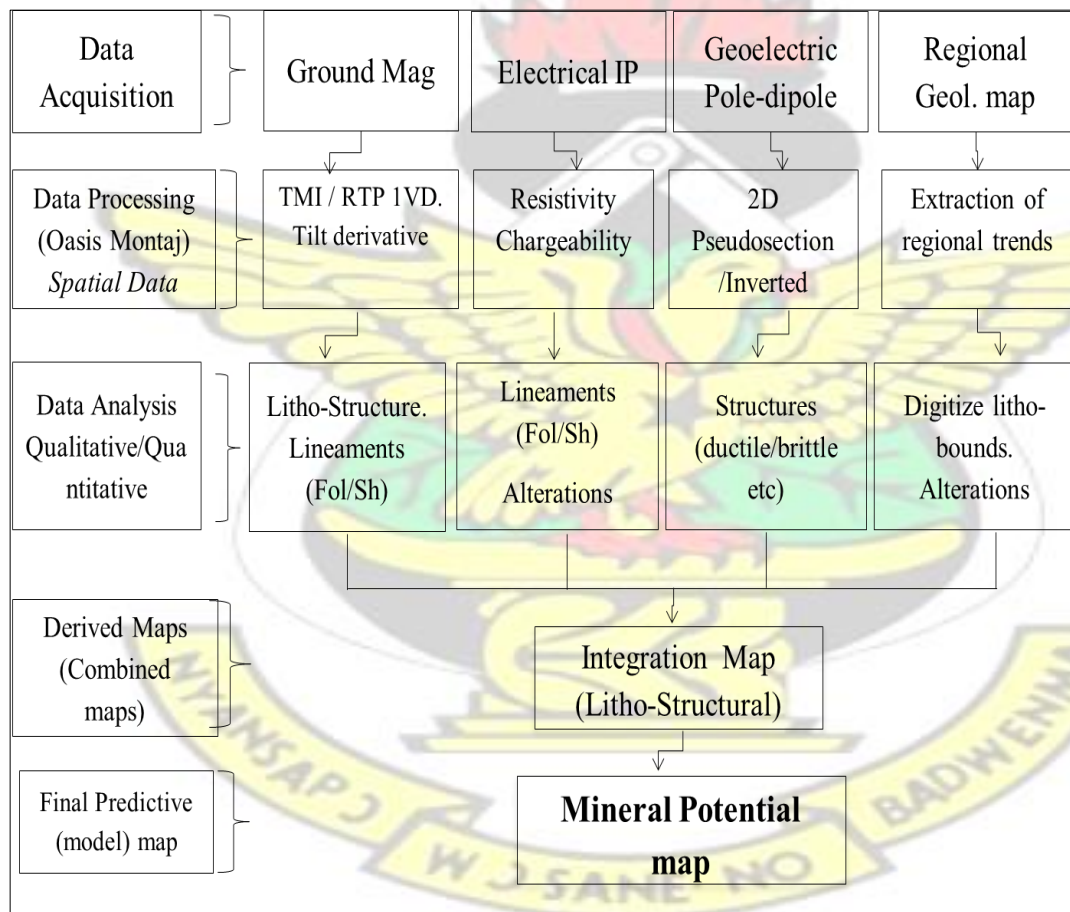


Figure 4.1: Flowchart of the methodology

4.2. Data source

The ground magnetic and geoelectric data were collected by Newmont's geophysics team during its ambitious gold prospecting campaign in 2010 on the Sefwi belt. The geophysical prospecting was a follow-up to a successful soil geochemistry program on the property. The study was conducted along a 3 km NE-SW traverse line and 1 km length cross-lines (sampling point) across the strike of the regional structural trend.

The survey was done using local coordinates for consistency, except the magnetic survey which was equipped with a GPS. The survey was subsequently transformed on to a Universal Transverse Mercator (UTM) projected coordinate system, Northern Hemisphere on World Geodetic System 1984 (WGS-84), zone 30 datum.

4.2.1. Ground Magnetic Metadata

The survey was conducted along sixty profile lines covering about three kilometers squared area. The surveyed grid was partitioned into blocks in order to enhance and speed up the data acquisition. Three blocks of 1 km² in each block. The base station was set up at a suitable place within the grid devoid of any cultural noises-rails, roofing sheets, metal fences etc. The base station was synchronized with the rover unit and tuned to the desired magnetic intensity of 32,000 nT with a cycling time of fifteen seconds. The rover was used for the field measurement at an automatic sampling rate of 1sec along 50 m line spacing. One of the quality control protocol ensured was to acquire the data before sun rise or noon, where diurnal effect is enormous. Consequently, all the data validation and cleaning was done on the raw data and prepared for processing.

4.2.1.1. Data Enhancement

The data was uploaded by magmap and imported into the Geosoft software and interpreted with the ArcGIS platform. All preprocessing corrections such as data checking and editing, diurnal removal, micro-leveling was carried out on the data. Next is the removal of Geomagnetic reference field from the data after tying-in the base-rover readings. The International Geomagnetic Reference Field (IGRF) is generally used for this purpose.

Additionally, some filtering techniques based on mathematical models were applied on the gridded data before post processing. The data was firstly imported in XYZ format into Geosoft database. Cleaning and data editing was achieved to remove cultural and other undesirable noises. Subsequently, the data was filtered to remove subtle noises or spikes. Non-linear filtering technique within Geosoft is an algorithm that is a noise-rejection filter. It is effective in eliminating geologic features of short wavelength, that is signal resulting from surficial features.

4.2.1.2. Gridding

Fifty thousand five hundred and six (50,506) stations were measured with the Geometrics 859 magnetometer. The diurnally corrected magnetic data was gridded using minimum curvature statistical tool, of a grid cell size of one fourth of line spacing. In this technique, the data is interpolated by a two dimensional surface to the raw XYZ data. This is accomplished in a way until the curvature of the surface is minimized. According to Briggs (1974) minimum curvature tool is now a common and popular gridding algorithm for analyzing data. However, O'Connell et al., (2005), until recently, developed an extension of the minimum-curvature-gridding algorithm

to address other challenges in data analysis. The result is a Total Magnetic Intensity (TMI) magnetic anomaly map.

4.2.1.3. Magnetic data filtering

The commencement of the interpretation of magnetic data to a large extent relies on the application of mathematical filters to observed data. Generally, the goal is to enhance the anomaly of interest and carefully retrieve information of the magnetization sources or location.

Oasis in-built MAGMAP tool possesses a powerful mathematical imaging technique that supports the application of two dimensional Fast Fourier Transform (2D-FFT) filters to gridded data. In this research, the MAGMAP filters that were used in the enhancement process included the upward-downward continuation, reduced to pole (RTP), first order derivative and tilt-angle derivation.

4.2.1.3.1. Upward-Continuation

Kellogg et al., (1953) emphasized that magnetic data measured can be transformed onto a reduced or higher elevation of the same data, thus over emphasizing shorter wavelengths anomalies or attenuating them. His algorithm tends to remove surficial noise. Because upward continuation does not produce any known side effect to the measured data, it is considered as a clean filter. That means the transformed data may not require further involvement of other filters or processes to correct them. Because of this, it is mostly utilized in removing or minimizing the effects of noise and shallow sources in grids. Magmap 1 step filter tool allowed the gridded data to be 5 m upward continued from the ground datum. It was applied on the TMI gridded map.

Upward continuity is given as:

$$L = e^{-hr} \quad (4.1)$$

h the distance in ground units r wavenumber (radians/ground unit). Note: $r = 2\pi k$ where k is cycles/ground unit.

4.2.1.3.2. Reduced to pole and equator

The causative body at depth is dependent on the shape of the magnetic anomaly. This definition is valid for both gravity and magnetic anomalies. However, the gravity and magnetic anomalies differ with the latter also dependent on the declination and the inclination of the magnetizing body. It is also dependent on the declination and inclination of the earth's local magnetic field and also the orientation or bearing of the body with respect to the magnetic north. Reduced to magnetic pole filter transforms an observed magnetic anomaly at any given location into the anomaly that would appear to have been taken at the North Pole. This algorithm was proposed by Baranov (1957) and Baranov and Naudy (1964) and was primarily meant to simplify the shape of the anomaly.

However, in this research the data was transformed to the equator since the study area is close to the equator. The concept of reduction to magnetic equator is given as

$$L(\theta) = \frac{[\sin(I) - i \cdot \cos(I) \cdot \cos(D - \theta)]^2 \times (-\cos^2(D - \theta))}{[\sin^2(I \alpha + \cos^2(D - \theta))] \times [\sin^2(I) + \cos^2(I) \cdot \cos^2(D - \theta)]} \quad (4.2)$$

where

I is the geomagnetic inclination (computed from projected –longitude/latitude data)

D is geomagnetic declination (computed from projected –longitude/latitude data)

$I\alpha$ is amplitude inclination correction which is never less than I . The projected data was transformed into geographic (longitude and latitude) and averaged for use in IGRF script in Oasis Montaj. The result yielded Inclination of minus 13.966, declination, minus 4.9 and field strength of 32046.26 nT. These parameters were used in the Magmap 1 step filtering to compute the reduce-to-magnetic equator anomaly. The resultant anomaly was transformed by multiplying the reduce-to-equator grid by a negative one thus flipping the anomalous colours.

4.2.1.3.3. First vertical derivative

The first vertical derivative (1VD) is a high pass filter that is applied to the total magnetic field data to calculate its gradient vertically. It has the effect of sharpening the higher frequency (short wavelength) magnetic features. It is also useful for enhancing the textural variation in the data. Vertical Derivatives are also known as vertical gradients (1VG / 2VG) can be generated from both TMI (and RTP) data.

Again the Magmap 1 step filtering tool was used in deducing 1VD signatures. Consequently, the RTP grid was visualized by displaying it in grey-shaded colour grid image within Grid and Image tool. One of the useful ways in recognizing structural trends and textural features is by displaying 1 VD in greyscale.

4.2.1.3.4. Tilt angle derivation

The total horizontal as well as the tilt derivatives is extremely useful in mapping out mineral exploration targets as well as shallow basement structures. The tilt derivative introduced by Miller and Singh (1994) and later by Verduzco et al., (2004) is defined as:

$$TDR = \tanh^{-1} \frac{1VDR}{THDR} \quad (4.3)$$

where 1VDR is the first order vertical derivative, THDR is the total horizontal derivative and T is the total magnetic intensity.

$$1VDR = \frac{\partial T}{\partial z} \quad (4.4) \text{ and}$$

$$THDR = \sqrt{\left(\left(\frac{\partial T}{\partial x}\right)^2 + \left(\frac{\partial T}{\partial y}\right)^2\right)} \quad (4.5)$$

Hence, tilt angle and the total horizontal derivatives introduced by Cooper and Crown (2006) can be summarized as

$$HD_TDR = \sqrt{\left(\left(\frac{\partial TDR}{\partial x}\right)^2 + \left(\frac{\partial TDR}{\partial y}\right)^2\right)} \quad (4.6)$$

The Total Horizontal Gradient is a high pass filter that calculates the amplitude of the total horizontal gradient vector of the magnetic field. The filter is essentially an edge detection (contact) filter and usually applied on both reduce to magnetic pole and equator anomaly. On the other hand, the complex analytical signal (Thurston and Smith, 1997) can be defined as:

$$T(x, y, z) = |A|esp(j\phi) \quad (4.7)$$

where

$$\phi = \tanh^{-1} \frac{(\partial T / \partial z)}{(\partial T / \partial x)} \quad (4.8)$$

$$|A| = \sqrt{\left(\frac{\partial T}{\partial x}\right)^2 + \left(\frac{\partial T}{\partial y}\right)^2 + \left(\frac{\partial T}{\partial z}\right)^2} \quad (4.9)$$

Where T is the Total Magnetic Intensity, |A| is the Analytical Signal, ϕ is the local phase, $\partial T / \partial z$ is the vertical derivative and horizontal derivatives are $\partial T / \partial x$ and $\partial T / \partial y$.

4.2.2. Gradient Resistivity and Induced Polarization

Geoelectric (IP/Resistivity) surveys were carried out on the same survey grid to that of the ground magnetic survey. The surveys were carried out using an Elrec Iris equipment. The instrument was connected to a series of potential electrodes of copper in copper sulphate solution. The current electrodes were set out using an aluminum foil as a contact material buried in wet earth material. This provided adequate low resistance of ground contact. Spatial coordinates were picked at 50 m interval within each block traversed, at an accuracy of ± 1 m.

At about 1000 m from the center of each block, current electrodes were placed at an AB = 200 m and potential electrode separation at 25 m was fixed as a sampling interval. Using an alternating square wave pulse via dual current electrodes, the ground surface is energized using the time domain IP technique.

The IP-resistivity measurements were made on a grid of regular stations along survey profile lines as with most acquisitions. The IP effect is measured as a time diminishing voltage at the electrode receivers after the transmitter (Tx) pulse has been emitted into the ground through the current electrodes.

4.2.3. Gradient Resistivity / IP data processing

The resistivity and chargeability data were recorded automatically by Elrec pro receiver. The data were subsequently imported into Prosys II, data management tool which allows data transfer files acquired in standard mode or in Multi-Electrode mode into spreadsheet format readable by Geosoft. The process involves downloading, importing into .csv or .txt file, visualizing (numerical or graphical), processing

(validation) and finally exporting into recognizable format to be post processed by Geosoft or Res2dinv software.

4.2.4. Gradient Resistivity / IP Qualitative map

The qualitative interpretation of gradient resistivity/chargeability was carried out on each block. A total of 4,958 data points were acquired for the three blocks and processed using Geosoft Oasis Montaj. The data was gridded using „Grid and Image“ tool in Geosoft. For the data values obtained, it was subjected to a minimum curvature surface algorithm which is the smoothest technique that fit the set of data.

This estimate is based upon the inverse distance average of the actual data within a specified search radius. The average of all the data points is used if there is no data within that radius of the grid. Additionally, to fit the actual data point nearest the coarse grid nodes, an iterative method is then utilized. Chargeability and measured resistivity channels are gridded separately. A grid cell size of 12.5 (1/4th line spacing), 99% pass tolerance, 100 iterations were chosen as parameters for the minimum curvature grid. The result is a resistivity and chargeability distribution map.

4.2.5. Pole-dipole geoelectric section

Two pole-dipole profiles (Line 21500 and Line 22700) were carried out at the northern and central portions of the study area. The pole-dipole configuration required a remote current electrode, C_2 (infinity), which is placed sufficiently far from the survey line. The other current electrode, C_1 was moved collinearly with the potential electrodes, P_{1-11} . In this study, an electrode spacing of 50 m was adopted to investigate shallow and deep structural features. The depth of penetration is 200 m.

4.2.6. Pole-dipole data processing

Pole-dipole data processing follows same procedure to that of gradient method; data import, visualization, validation and exporting to Geosoft or Res2dinv software. Pole dipole is a form of qualitative interpretation of the gradient survey. Pole-dipole lines that were surveyed superimposed on the gradient array data and provide a 2D section information along surveyed lines.

Apparent resistivity plot was achieved by the use of Geosoft in-built Pseudo-section plot tool was used to select chargeability and resistivity channels to plot, as well as gridded section data to display on section. Apparent resistivity pseudo-section checks for erratic manner of high and low values, which are related to noise! Similarly, an erratic pattern in IP values denotes noisy apparent IP pseudo-section signature.

4.2.7. Pole-dipole Inverse model

The pole-dipole data were further processed and interpreted by the use of the Res2dinv (Loke, 2003) software tool. Based on set of mathematical algorithm rules, the result obtained would be an interpretable image of the electrical resistivity and chargeability distribution in the subsurface. Although inversion and modeling processing remains highly subjective, they have recently become available and versatile in huge data processing and allow a more definitive interpretation.

The purpose of the inversion and modeling processes is to transform apparent chargeability and resistivity measurements into a true “Interpreted Depth Section.”

The 2D inversion model contains of a number of rectangular cells whose arrangement approximately follows the distribution of the data points in the apparent resistivity pseudo-section. In the present study, the obtained data have undergone

several processing steps through the RES2DINV software to produce a smooth model. An initial damping factor of 0.16 and minimum damping factor 0.015 were used. The unit of electrode spacing is the same as the width of the interior model cells.

4.2.8. Model Theory

The theory model behind the inversion program is based on the smoothness-constrained least-squares method (de Groot-Hedlin and Constable 1990, Sasaki 1992, Loke et al. 2003). The following equation underscores the smoothness-constrained least-squares method

$$(J^T J + \lambda F) \Delta q_k = J_g^T - \lambda F_{qk} \quad (4.1)$$

$$F = \alpha_x C_x^T C_x + \alpha_z C_z^T C_z \quad (4.2)$$

where

C_x is the horizontal roughness filter

C_z is the roughness filter in the vertical direction

J is the Jacobian matrix of partial derivative J^T

is transpose of J

λ is the damping factor g and q are data misfit vector and model change vector respectively. By adjusting the resistivity of the block model subject to smoothness constrained used, the optimization method would attempt to minimize the difference between the measured apparent resistivity values. The root-mean-squared (RMS) error is the measure of this difference. However the model with the lowest possible RMS

error can sometimes show large and unrealistic variations in the model resistivity values. From geologic perspective, this might not always be the "best" model. Choosing a model at the iteration after which RMS error would not change significantly is the most prudent approach and this best occur between 3rd and 5th iterations.

4.2.9. Pole-dipole Quantitative map

The raw data was processed with Oasis Montaj's pseudo-section tool. The plotted pseudo-sections represent apparent information. However, upon inversion with Res2dinv (Loke, 2003), the data was inverted to real resistivity and chargeability 2d sections. Real dips are recognized in section.

They are helpful in showing the direction and plunge to plan drill hole orientation and planned depths to intercept potential target zones.

CHAPTER FIVE

RESULTS AND DISCUSSIONS

This chapter deals with the integration of magnetic, geoelectric datasets and existing regional geological map to generate interpretive geological map. This involves the use of GIS-based tools to seek out trends and patterns that will help characterize, understand and predict local structural features.

5.1. Digital elevation map

Elevation column extracted from the ground magnetic datasets was used to create a digital elevation map using Surfer 11. A total of 52,552 data points were gridded using minimum curvature of grid size 100 rows x 82 columns. Figure 5.1 shows a 3D surface

which shows the elevation of the study area to be extremely undulating and range from 150 m to 230 m above mean sea level. The high-lands trends NE-SW being truncated by three valleys and occupies about two-thirds of the entire study area. The highest peak is at 246 m above mean sea level (MSL).

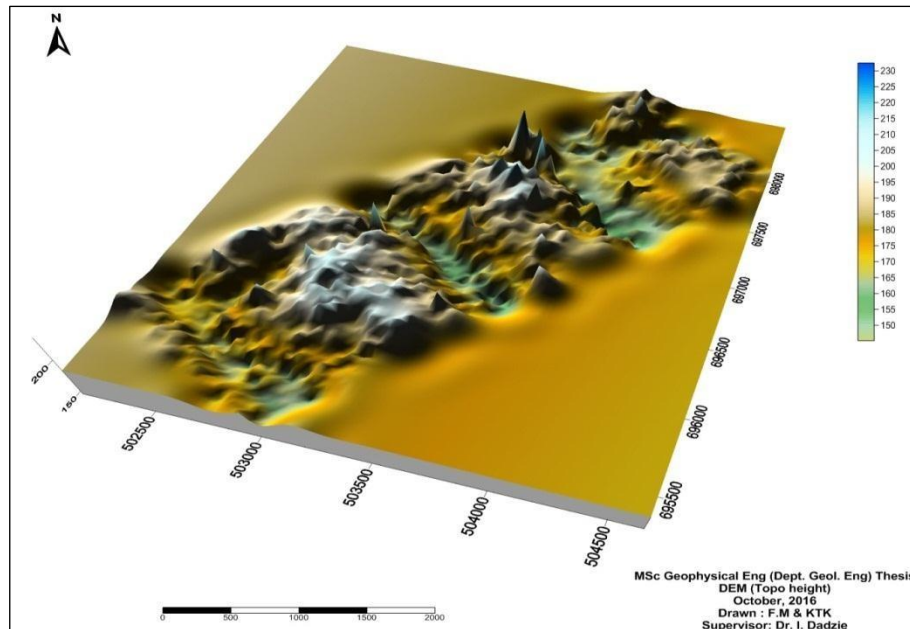


Figure 5.1: 3D surface DEM of study area

5.2. Mapping of structural features

The aim of this section is to help improve on the existing geological map and to reduce the level of subjectivity related to geophysical interpretation. The work will further attempt to map out structural indicators from geophysical signatures obtained from the field datasets and the use of various GIS-based tools to extract them into mappable units. Four main important indicative spatial features or exploration guides were used to characterize structural trends related to potential auriferous zones;

- shear zones related to ductile or contacts
- favorable host rock units with fracture arrays, stockwork or brecciated zones

- hydrothermal alterations and
- strongly deformed or faults zones

5.3. Qualitative Interpretation

The present interpreted geological map underlain for this work comprises of three main features or lithologies;

- GR- Belt type granitoid, mainly hornblende dominated, granodiorite and diorite
- BS- Lower Birimian meta-sediments series or sediments, mainly of phyllites, greywackes, schists and tuffs
- BV- Upper Birimian series, mainly meta-volcanics and volcanoclastics.

5.3.1. Interpreting Lithological units

Reduced to pole map was used to delineate lithological units exclusively and three responses were identified; low, intermediate and high magnetic responses. The magnetic signature also be grouped further into very low (-2.0 to -34 nT), fairly smooth positive (10 to 90 nT) and high positive (95 to 180 nT) susceptibilities. The bedrock or host rock is interpreted as Birimian sediments due to its very low susceptibility as in Figure 5.2.

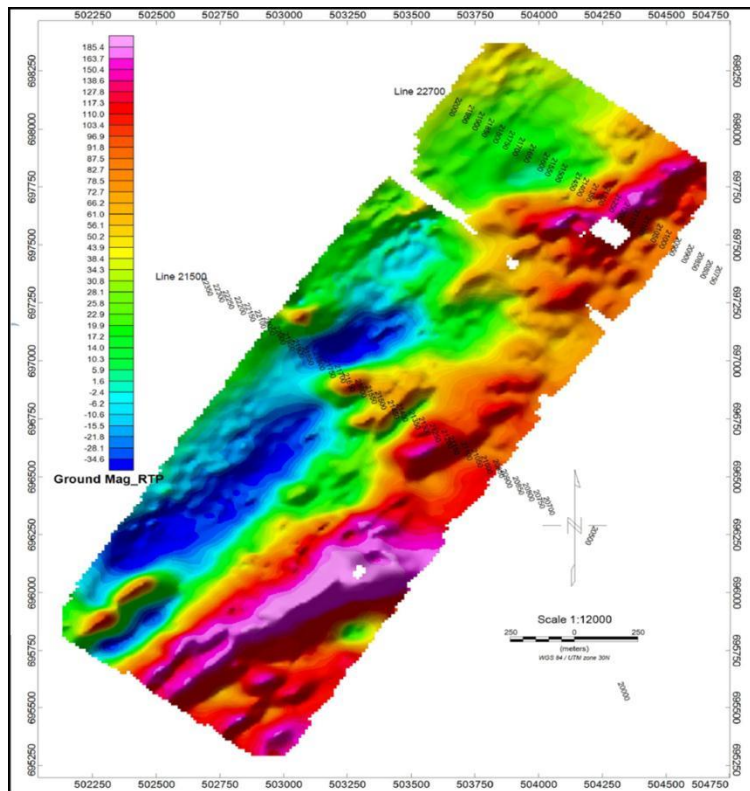


Figure 5.2 Interpreting lithological units from RTP magnetic anomaly

Belt type intrusive unit was classified into three distinct groups as GR1 to GR3 (Figure 5.2). The main lithological units generally trends NE-SW direction. Extraction of favourable geologic units from the magnetic signature agrees with the existing geological map.

However, improved resolution of the magnetic signature has been useful in delineating in detail the geological formation against the background of regional trend. Resolving lithological contacts was challenging with the resistivity and chargeability anomaly map. The data resolution in electrical survey is less desirable than in magnetic data. This is because geoelectric survey utilizes about four times line spacing far larger than in magnetic survey.

5.3.2. Structural interpretation

Identification of lineaments is a key to structural analysis which is considered as trap zones and conduits for mineralization fluids. In this work, lineaments are grouped into shear zones (extensional vein systems) and fractures (foliations and cleavages). Magnetic susceptibility of rock forming minerals is generally low in intensely fractured or deformed rock units.

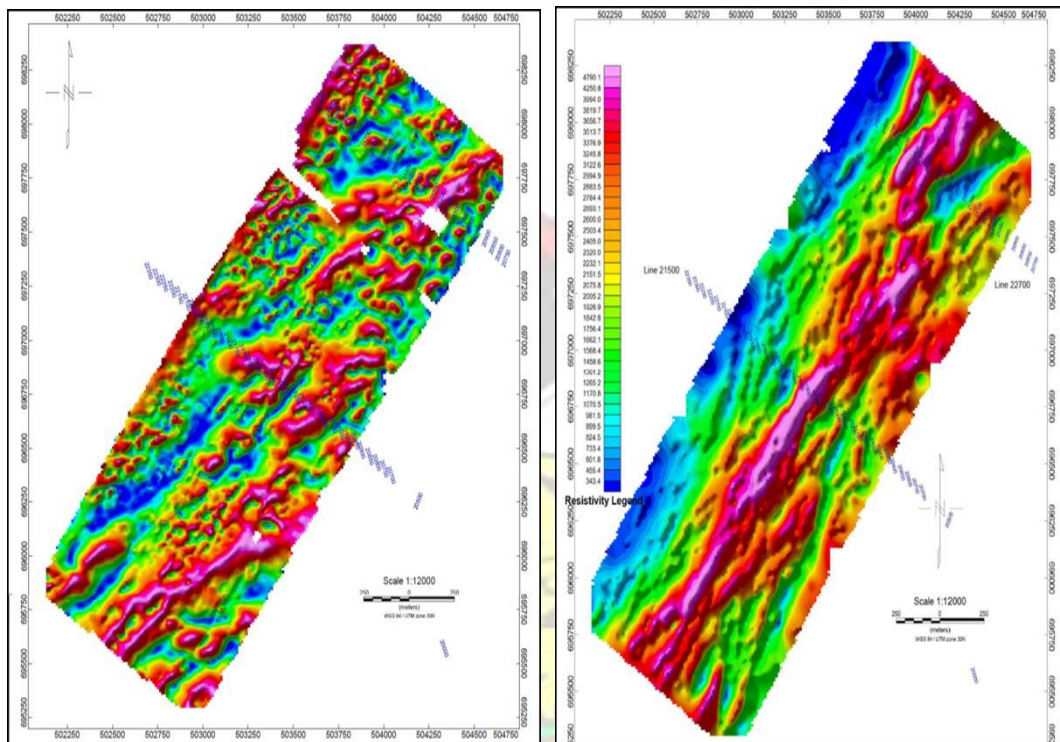


Figure 5.3 Tilt derivative and resistivity anomalous map

This is because all ferrimagnetic minerals are destroyed or metamorphosed into other lithological units of lower magnetic susceptibilities. This phenomenon formed the basis for magnetic lineament interpretation of this project. On the other hand, the decrease in electrical resistivity of rocks is as a result of significant increase in clay minerals, alteration or fracture frequency.

A coloured-shaded map of tilt derivative and resistivity anomalous maps are presented in figure 5.3. Lineaments were largely extracted from these anomalous maps and 1 VD signature in appendix. The tilt derivative (TDR) of the magnetic field was created to

increase the chances of or to facilitate magnetic lineaments identification. The main objective of the tilt derivative is to enhance subtle anomalies by normalizing the magnetic field. It can be linked to the automatic gain control filter.

A total of one hundred and forty four magnetic lineaments were extracted from the tilt derivative and two hundred and thirty four from the 1 VD anomalies. Most of the shear lineaments were obtained from the 1 VD spatial map. Furthermore, all lineaments were coordinated and linked into one single lineament map. The subjectivity of the coordination may vary due to the judged level of visibility and resolution of the anomalous map. The different datasets and the data resolution have marked variations that resulted in marked variation in the positioning of the lineaments.

It is seen that, the structural features trend NE-SW in the linked 1VD/resistivity map (Figure 5.4). However, the tilt derivative showed an erratic feature indicating high degree of structural deformation which may be related to shearing.

These structures can be grouped as

- boudins and boudinage: this is due to extensional deformation applied to rock formation made of alternating stronger and less strong layers. They result in the development of pinch and swell structures.

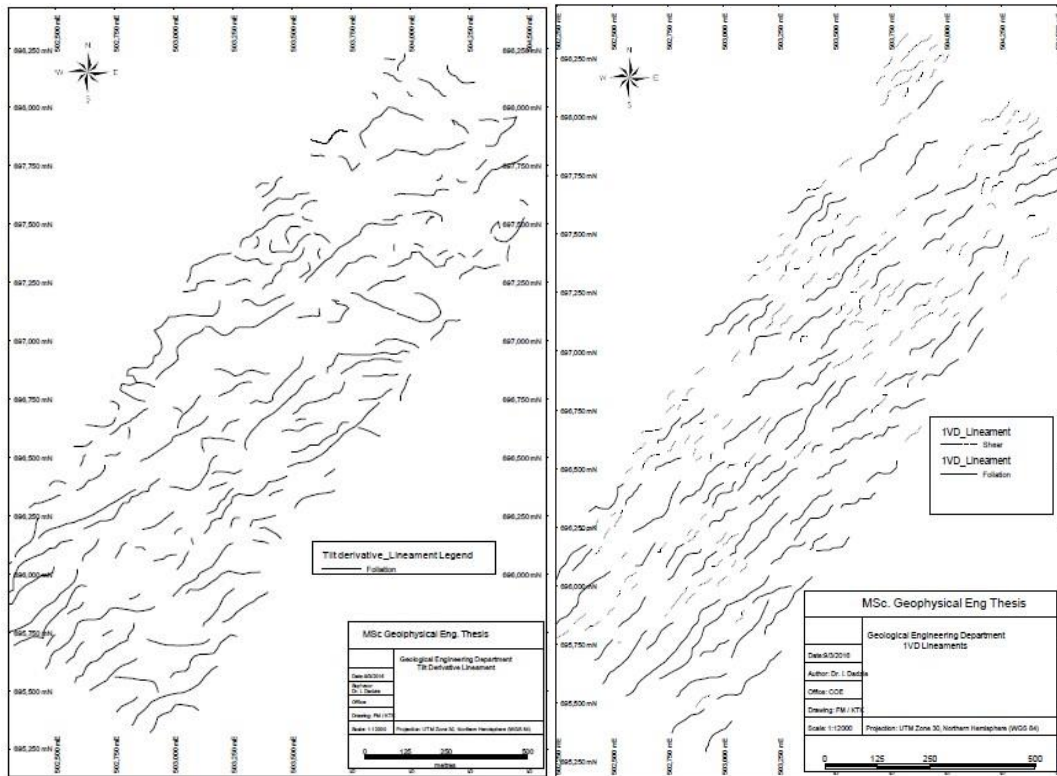


Figure 5.4: Tilt angle lineament (foliation) and 1 VD shear/foliation lineaments

- ductile shear zones: these are as a results of slow, progressive deformation over long period of time. These can develop into S_1 foliation planar fabric, analogous to cleavage plane in folds
- schistosity : which occurs from the ductile flattening of grain aggregates (eg quartz) or change in orientation of tabular minerals (eg micas)

Extracted lineaments therefore were classified into two units, shear zones and fracture zones. In gold mineralization, the shear and fractured zones are linked to regional and local scale respectively. From the linked lineation map, therefore, it can be concluded that the area of interest is a favourable mineralization potential zone.

5.3.2.1. Pole-dipole Geoelectrical inversion

The modeling products came out good and the sections mapped features to up 200m below topography. The sections revealed all the big breaks in the competent rocks (granitoids/ volcanics). These fractured networks in competent rocks serve as conduit for hydrothermal fluids (Figure 5.5). Also the contacts of such big breaks (fault zones) are worth targeting.

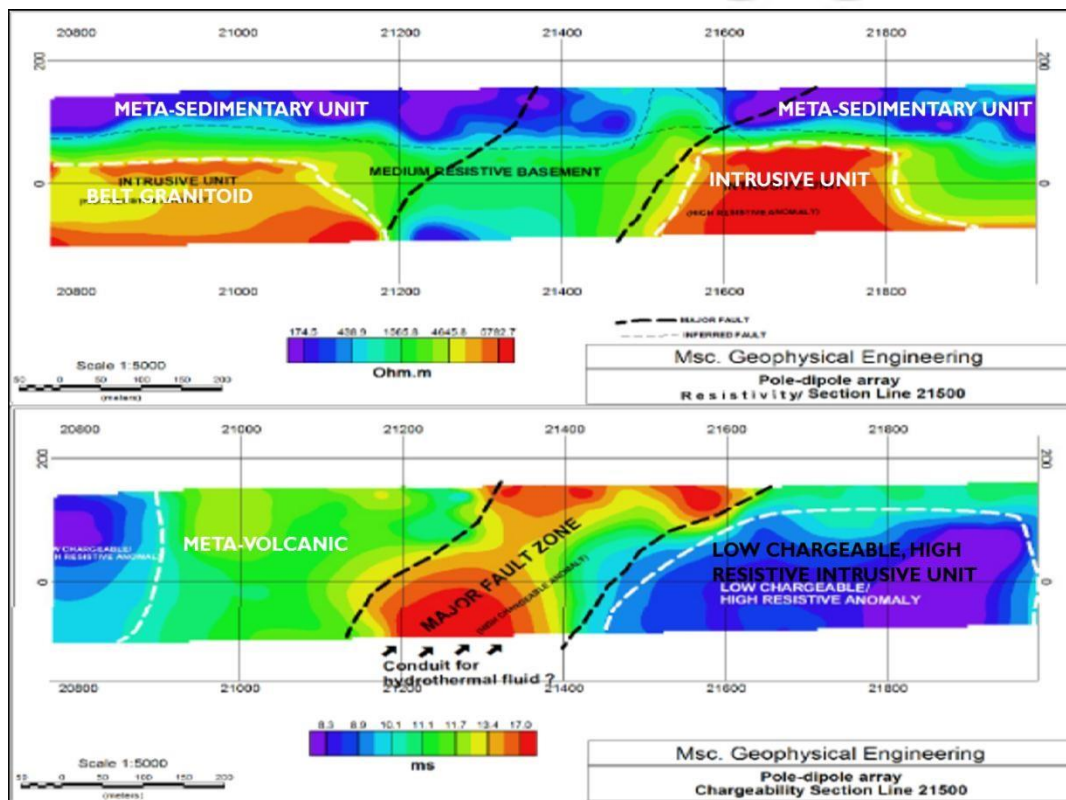


Figure 5.5 Pole-dipole section Line 21500

The pole-dipole section lines 21500 and 22700 provides a preliminary interpretation for the recognition of major structures and is located at the central and northern portion of the study area respectively (Figure 5.3). The geoelectrical section line 21500 in figure 5.5 shows a major conductive structure sandwiched between two major intrusive unit (high resistive packages).

The interpreted fault zone plunges at 045° and at an approximate width of 200m. The depth of this highly conductive zone is estimated at 200 m and likely at a deeper depth.

This major conductive unit may be interpreted as conduit for hydrothermal fluid and therefore a highly favourable zone to test for gold mineralization in a detail exploration campaign.

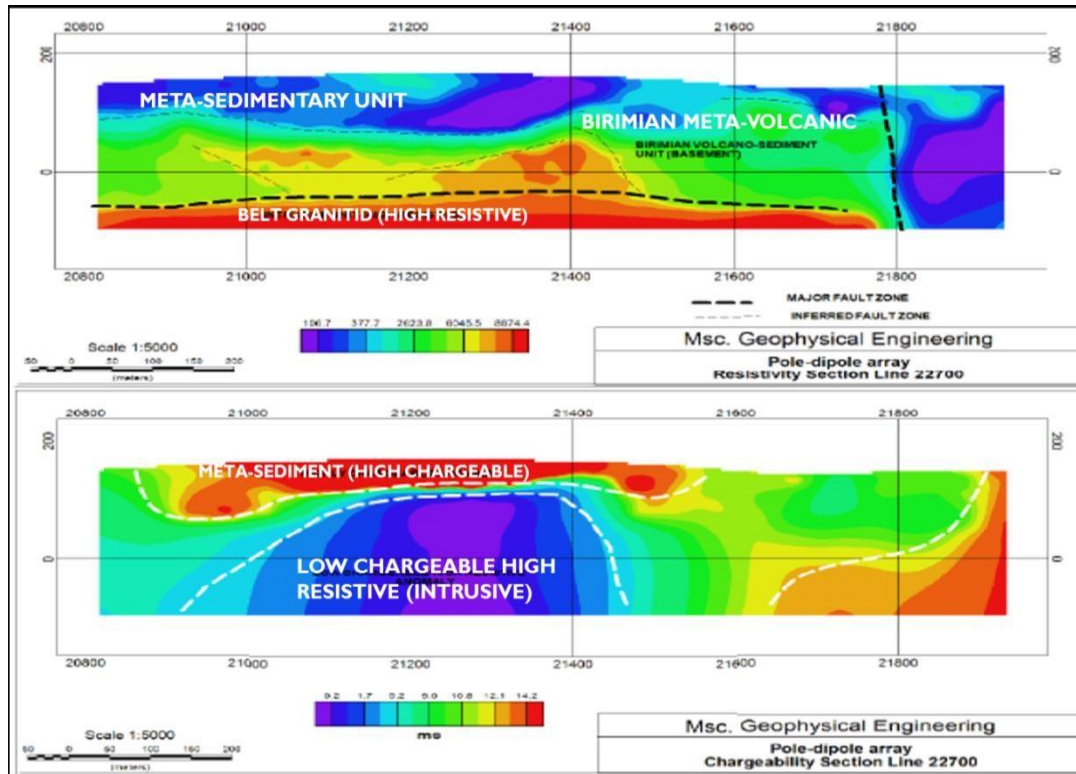


Figure 5.6 Pole-dipole section Line 22700

Several minor faults were inferred at low-high resistive boundaries though such minor faults are not widespread yet they play crucial role in the recognition of favourable mineralization potential. Figure 5.6 shows the geoelectrical section Line 22700 exhibiting several minor inferred faults at low-high resistive boundary. A highly resistive, deep seated (160 m below ground level) intrusive package is interpreted as belt granitoid is in conformity with the magnetic signature (Figure 5.2). Three distinct conductive anomalous zones are delineated from the IP-chargeability section results.

5.3.3. Extraction Alteration anomalies

The gradient IP map (Figure 5.7) shows low, medium to high chargeability anomalies trending NE-SW.

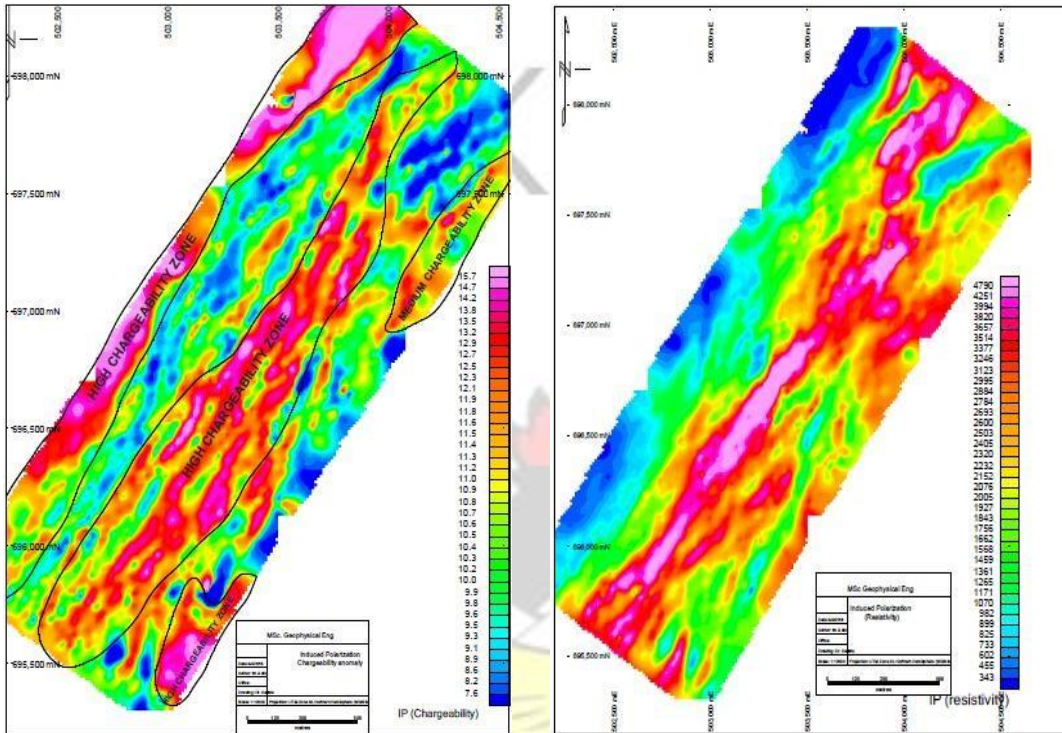


Figure 5.7 Alteration anomalies mapped from IP chargeability and resistivity signatures

The gradient resistivity map and IP-chargeability map (Fig. 5.7) reflects the same trend of low resistive and high chargeability trends as in figure 5.6. The high chargeability zone ranges from 10.0 - 15.7 VV^{-1} . Two chargeability anomalies clearly appear on the IP map which is quite conformable with the anomalies derived from the resistivity map but have somewhat less relief.

Two of such anomalies are very prominent and are situated in the central and the western flank of the study area. The central anomaly sits conformably on a highly resistive anomaly and is interpreted as silicified (or felsic intrusive) units with disseminated metallic oxides (pyrite, arsenopyrite, pyrrhotite). On the western flank is marked high chargeability on a low resistive package (Figure 5.5) which may be

interpreted as weathered Birimian meta-volcano sedimentary unit (phyllite or meta greywacke).

The similarity in locating the geophysical anomalies on both maps gives a good support for the existence of near surface causative bodies (Loke and Barker, 1996) and could be economic interest. So, these results suggested that these locations must be followed by detailed geophysical survey measurements in order to locate metallic mineralization occurrences in the next stage.

5.4. Mineral potential map

The interpreted geological map shown in figure 5.8 is the result of mapping all structural trends obtained from the geophysical anomalies and existing geological map. The map exhibits alteration zones, lineaments and fault elements trending NE– SW direction. These clearly displayed in the first vertical derivative of the magnetic map (Fig. 5.2). Also the interpretation of the geophysical data indicates that these trends might be associated with alteration zones and have been preliminary interpreted as related to ore deposits at different depths. The interpreted geological map produced from this study comprises of NE-SW trend with a litho-structural configuration of Birimian meta-volcanosediment and belt granitoid units. The target includes two main cluster and minor anomalies with an aggregate strike length of 3 km. Geological interpretation carried out on section lines 21500 and 22700 revealed steeply dipping major fault, trending NE-SW and passing through the center of the study area.

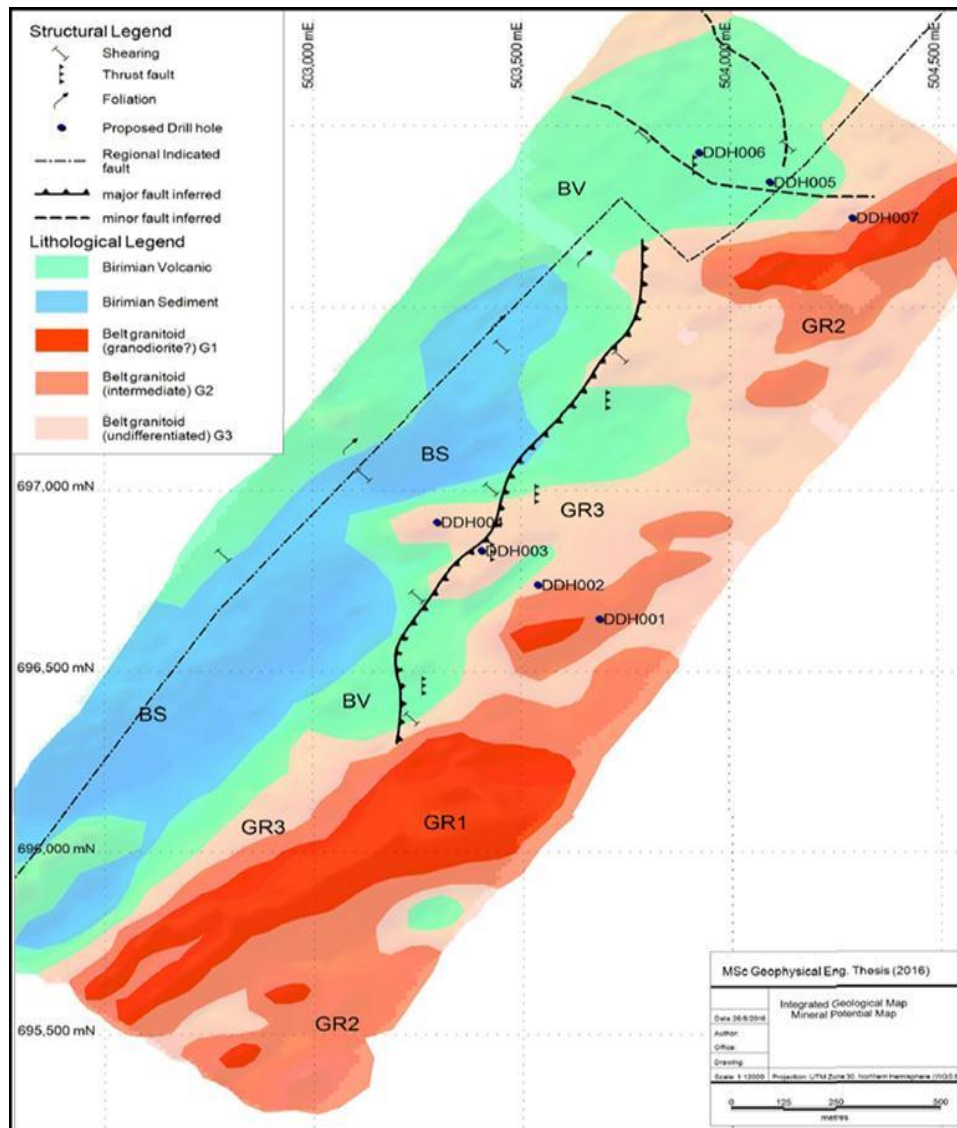


Figure 5.8 Interpreted detail geological and mineral potential map. This suggests that the contacts are structurally controlled and thus potential site for mineralization. There is an interplay of structural patterns (lineation and shearing) and may be interpreted as post thrust deformation (D2) events. Also, major thrust fault may be characterized by D3 deformational event and could be an interesting site for tectonic events.

Seven diamond drill holes (Table 5.1) are intuitively planned to test the reliability and the overall success of the interpreted geological map and also to ascertain missing “links” in the preliminary interpretation. Drill holes DDH001-007 would ultimately determine the depth of the resistive-chargeable anomalous units as well as litho-

structural boundaries (Figure 5.5). Further drill holes would be planned on the lateral profile of the main fault boundary in if the first-pass drilling becomes successful.

Table 5.1 Proposed diamond drill holes

ID	UTM East	UTM North	Prop Depth	Azimuth	Dip	Remark
DD01	503690	696645	150	110	-55	Test resist-chargeable at depth
DD02	503542	696739	180	110	-55	Same as D01. Test down dip of D03.
DD03	503406	696831	180	110	-55	Test major fault and down dip of D04
DD04	503300	696911	180	110	-55	Test litho-structural configuration
DD05	504095	697843	180	110	-55	Test minor fault and down dip of D07
DD06	503926	697925	180	110	-55	Test litho-structural configuration
DD07	504294	697745	180	110	-55	Test resist-chargeable at depth

CHAPTER SIX

CONCLUSION AND RECOMMENDATION

6.1. Conclusions

In conclusion the interpretation of the integrated magnetic, electrical and structural datasets within the Sefwi Belt of Ghana provides the area considered as a good location for the mineral ore occurrences and the geological structural situation of the area may be a controlling feature on the ore deposition. Detailed interpreted geological map was produced which reflects mineral potential map. The potential map produced is a high resolution map in stark contrast to aeromagnetic map generated in most regional geophysical surveys. The detailed map helped in delineating three major lithological units; Birimian sediments, Birimian volcanics and belt-type granitoid.

These geological formations were seen to trend in the NE-SW direction with a lot of structural deformation that correspond to the D1 and D2 syn or post deformational stages. Ground magnetic truthing contributed in mapping litho-structural trends as well as textural features related to lineaments. IP anomaly map focused on defining

alteration patterns of resistive-conductive boundaries which gives a unique interpretation of indicative of deep structures (good fluid conduits).

Integration of geophysical, structural datasets was key in high grade target and providing a preliminary interpretation on stratigraphy and structural orientations. The results of resistivity and IP inversions of pole-dipole data indicated that there are conductive and chargeable bodies at depths ranging from 50 to 200 m. This exploration model would be tested with the seven proposed diamond drill boreholes in order to ascertain the nature of the structural configuration and conductive and resistive anomalous trends. Finally, this research resulted in high resolution integrated map of the area, using geology and geophysical dataset and GIS-based software, hence it could be stated hypothetically, that Sefwi belt is highly a potential gold bearing belt.

6.2. Recommendations

It is recommended that ground base radiometric survey be carried out to delineate alteration packages which are responsive to hydrothermal processes. Trenching and pitting is recommended before the first-pass drilling campaign. This means geophysics should be incorporated at the earliest stages of exploration campaign.

Detailed geological mapping for structures, veining, alterations and mineralization and should always precede the sampling so that sample intervals can be established and analytical results can be more effectively interpreted. Again to quantify the geometry and nature of structural trends at depth, the study also recommends 3D inversion of the magnetic datasets. This would invariably enhance the objectivity of the structural setting.

REFERENCES

- Anderson L A 1984 Self-potential investigations in the Puhimau thermal area, Kilauea Volcano, Hawaii SEG Expanded Abstr. 3 84
DOI:10.1190/1.1894270.
- Archie, G.E. (1942) The electrical resistivity log as an aid to determining some reservoir characteristics. *Trans. A.I.M.E.*, 146: 389-409.
- Baranov, V., 1957, A new method for interpretation of aeromagnetic maps pseudogravimetric anomalies: *Geophysics*, 22, 359–383.
- Baranov, V., and H. Naudy, 1964, Numerical calculation of the formula of reduction to the magnetic pole: *Geophysics*, 29, 67–79.
- Barker, R.D. (1981) Offset system of electrical resistivity sounding and its use with a multicore cable. *Geophysical Prospecting*, 29(1): 128-143.
- Briggs, I. C., 1974, Machine contouring using minimum curvature: *Geophysics*, 39, 39–48.
- Broadbent, M. and Habberjam, G.M. (1971) A solution to the dipping' interface problem using the square array resistivity technique. *Geophysical Prospecting*, 19(3): 321-338.
- Boyle, R. W., 1979. *The Geochemistry of Gold and Its Deposits*. *Geol. Surv. Can. Bull.* 280, 584 p.
- Campbell, W. C., 1997, *Introduction to geomagnetic fields*: Cambridge University Press.
- Corry C E 1981 The role of the self-potential method in the exploration for molybdenite AMAX, Climax Molybdenum Co., Golden, CO, 53 pp (7 maps)
- Corwin R F and Hoover D B 1979 The self-potential method in geothermal exploration *Geophysics* 44 226–45.
- Cooper, G. R. J., and D. R. Cowan, 2006, Enhancing potential field data using filters based on the local phase: *Computers and Geosciences*, 32, 1585-1591.
- deGroot-Hedlin, C., Constable, S., 1990. Occam's inversion to generate smooth, twodimensional models from magnetotelluric data. *Geophysics* 55 (12), 1613-1624.

- Doell, R. and Cox, A., 1967. Magnetization of Rocks. In: SEG Mining Geophysics Volume Editorial Committee (Editors), Mining Geophysics, Volume 2: Theory. Society of Exploration Geophysicists, Tulsa pp. 446-453.
- Fon, A.N., Che, V.B., Suh, C.E., 2012.. Application of Electrical Resistivity and Chargeability Data on a GIS Platform in Delineating Auriferous Structures in a Deeply Weathered Lateritic Terrain, Eastern Cameroon. International Journal of Geosciences. <http://doi.org/10.4236/ijg.2012.325097>
- Griffis, R.J., Barning, K., Agezo, F.L., Akosah, F.K., 2002. Gold Deposits of Ghana, Minerals Commission, Accra, Ghana, 14-108.
- Groves D.I., Goldfarb, R.J., Genre-Mariam, M., Hagemann, S.G., and Robert, F., 1998, Orogenic gold deposits : A proposed classification in the context of their crustal distribution and relationships to other gold deposit types: Ore Geology Reviews, 13, 7-17.
- Gyngell, N.R., 1997. Second horizontal derivatives of ground magnetic data applied to gold exploration in the Yilgarn Craton of Western Australia. Exploration Geophysics 28: 232-234
- Haberjarm. G.M. and Watkins, G.E. (1967a) The reduction of lateral effects in resistivity probing. Geophysical Prospecting, 15(2): 221-235.
- Hagemann S.G., and Brown P.E., 2000, Gold in 2000: an introduction, in Society of Economic Geologists Reviews in Economic Geology 13, 1-7.
- Hanna, W. F., 1990, Some historical notes on early magnetic surveying in the U. S. Geological Survey, in W. F. Hanna, ed., Geologic applications of modern aeromagnetic surveys: U. S. Geological Survey Bulletin 1224, 63–73.
- H. Hase, T. Hashimoto, S. Sakanaka, W. Kanda and Y. Tanaka, “Hydrothermal System Beneath Aso Volcano as Inferred from Self Potential Mapping and Resistivity Structure,” Journal of Volcanology and Geothermal Research, Vol. 134, No. 4, 2005, pp. 259-278. doi:10.1016/j.jvolgeores.2004.12.005
- Hirst, T., 1938. The geology of the Tarkwa goldfield and adjacent country. Gold Coast Geol. Surv. Bull. 10, Accra. (out of print).
- Heureux, E. L., Ugalde, H., Qian, W., Milkereit, B., & Nasui, C. (2007). An integrated geophysical study for orebody delineation, (April), 37–40.
- Junner, N. R., 1932. 1943. The diamond deposits of the Gold Coast, with notes on other diamond deposits in West Africa. Gold Coast. Geol. Surv. Bull. 12 (1943)

and 1958 editions out of print) Poulsen, K.H., Robert, F., and Dubé, B., 2000, Geological classification of Canadian gold deposits: Geological Survey of Canada Bulletin 540.

Kearey Philip, Michael Brooks, Ian Hill. (2002). An Introduction to Geophysical Exploration Third Edition. Osney Mead, Oxford OX2 0EL: Blackwell Science Ltd.

Kiberu J 2002 Induced polarization and resistivity measurements on a suite of near surface soil samples and their empirical relationship to selected measured engineering parameters MSC. Thesis International Institute for Geoinformation Science and Earth Observation (ITC), Enschede, The Netherlands p 119.

Loke, M. N. and Barker, R. D. 1996 a: Rapid leastsquares inversion of apparent resistivity pseudosection using aquas:- Newton method. Geophysics prospecting, Vol. 44, p 131-152.

Loke, M.H., Electrical Imaging Survey for Environmental and Engineering Studies: A Practical Guide to 2-D and 3-D Survey. USM, Penang, Malaysia, (2003).

Lowrie, W. (1990) Magnetic analysis of rock fabric. In: James, D.E. (ed.), The Encyclopedia of Solid Earth Geophysics. New York: Van Nostrand Reinhold, 698-706.

Macnae J C 1979 Kimberlites and exploration geophysics Geophysics 44 1395-416

Merrill, R.T., McEhinny, M.W. and McFadden, P.L., 1996. The magnetic field of the earth: paleomagnetism, the core and the deep mantle. Academic Press, San Diego, 531 pp.

Miller, H. G. and Singh, V., 1994, Potential Field Tilt – a new concept for location of potential field sources: Journal of Applied Geophysics, 32, 213-217.

Milligan, P.R. and Gunn, P.J., 1997. Enhancement and presentation of airborne geophysical data. AGSO Journal of Geology and Geophysics 17: 63-75.

O'Connell, M. D., R. S. Smith, and M. A. Vall' ee, 2005, Gridding aeromagnetic data using longitudinal and transverse gradients with the minimum curvature operator: The Leading Edge, 24, 142-145.

Ramadan T M and Sultan A S 2004 Integration of remote sensing, geological and geophysical data for the identification of massive sulphide zones at Wadi Allaqi area Middle East J., Ain Shams Univ., Earth Sci. Ser. 18 165-74

- Poulsen, K.H., Robert, F., and Dubé, B., 2000, Geological classification of Canadian gold deposits: Geological Survey of Canada Bulletin 540
- Reford, M. S., and J. S. Sumner, 1964, Aeromagnetism: *Geophysics*, 29, 482–516.
- Robert, F., Brommecker, R., Bourne, B., Dobak, P., McEwan, C., Rowe, R., & Zhou, X. (2007). Models and Exploration Methods for Major Gold Deposit Types. In *Proceedings of Exploration 07: Fifth Decennial International Conference on Mineral Exploration* (Vol. 48, pp. 691–711).
- Robert, F., 2004a, Geologic footprints of gold systems, in J Muhling et al. eds., *SEG 2004: Predictive Mineral Discovery Under Cover, Extended Abstracts: Centre for Global Metallogeny, The University of Western Australia Publication 33*, 97-101.
- Robert, F., Poulsen, K.H., 2001, Vein Formation and Deformation in greenstone Gold Deposits, in *Society of Economic geologists, Reviews in Economic Geology* 14, 111-155.
- Robert, F, Poulsen, K.H., and Dubé, B., 1997, Gold deposits and their geological classification, in A.G. Gubins, ed., *Proceedings of Exploration'97: Fourth Decennial International Conference on Mineral Exploration*, 209-220.
- Sam, T. B. F., 1898. On the origin of auriferous conglomerates of the Gold Coast Colony (West Africa). *London Quart. Jr. of the Geol. Society*, vol. 44, p. 290.
- Sasaki, Y., 1992, Resolution of resistivity tomography inferred from numerical simulation. *Geophysical Prospecting* 40 (4), 453-464.
- Sestini, G., 1973. Sedimentology of a paleoplacer: the gold bearing Tarkwaian of Ghana; in Amstutz, G. C. and A. J. Bernard (Eds): *Ores in Sediments*, pp. 275-305, Springer-Verlag, Heidelberg.
- Sheriff, R. E. T. W. M. G. L. P. (1928). *Applied Geophysics*. Science (New York, N.Y.) (2nd ed., Vol. 67). Cambridge: Cambridge University Press.
<http://doi.org/10.1180/minmag.1982.046.341.32>
- Smith R J 2002 *Geophysics of Iron Oxide Copper-Gold Deposits (Hydrothermal Iron Oxide Copper–Gold and Related Deposits: A Global Perspective vol 2)* ed T M Porter (Adelaide: PGC Publishing) pp 357–67.
- Telford, W.M., Geldhart, L.P., Sheriff, R. E. (2004). *Applied Geophysics* (2nd ed.). Cambridge: Cambridge University Press, 75-90.
- Telford, W. M., L. P. Geldart, and R. E. Sheriff, 1990, *Applied geophysics*, 2nd ed.: Cambridge University Press.

Telford, W.M., Geldart, L.P., Sheriff, R.E. and Keys, D.A., 1976. Applied Geophysics. Cambridge University Press, Cambridge, 860 pp.

Thompson, D.T. (1982) EULDPH: a new technique for making computerassisted depth estimates from magnetic data. Geophysics, 47(1): 31-37.

Thurston, J.B., and Smith, R.S., 1997, Automatic conversion of magnetic data to depth, dip and susceptibility contrast using the SPITM method, Geophysics, v. 62, p. 807-813

Verduzco, B., J. D. Fairhead, C. M. Green, and C. Mackenzie, 2004, New insights into magnetic derivatives: The Leading Edge, 22, 116–119, doi:10.1190/1.1651454.

Yungul S 1950 Interpretation of spontaneous polarization anomalies caused by spheroidal ore bodies Geophysics 15 237–46

www.ghanadistrict.com, © 2006. A Public - Private Partnership Programme between Ministry of Local Government and Rural Development and Maks Publications & Media Services



APPENDICES

APPENDIX A

Appendix A. 1 : Ground magnetic data processed for Diurnal correction

Line	READING (nT)	Diurnal_ (nT)	RL	Long	Lat	UTM_East	UTM_North
L2135	32182	3.26	165	-2.97167	6.30415	503133	696827
0L2050	32220	42.88	184	-2.97552	6.297505	502708	696092
0L2125	32226	43.11	185	-2.97151	6.303026	503152	696702
0L2125	32186	3.22	166	-2.96971	6.301697	503350	696554
0L2045	32225	43.11	176	-2.97643	6.297531	502607	696095
0L2045	32225	42.81	178	-2.97635	6.297492	502616	696091
0L2045	32212	42.81	189	-2.97584	6.29712 ⁵	502672	696049
0L2120	32215	43.09	179	-2.97094	6.30196	503215	696584
0L2040	32266	80.24	186	-2.97779	6.297942	502457	696140
0L2110	32227	43.11	190	-2.97087	6.30078 ⁶	503222	696454
0L2110	32226	42.81	188	-2.97092	6.30081	503216	696457
0L2110	32227	43.11	192	-2.97125	6.301062	503180	696485
0L2030	32195	3.15	168	-2.97728	6.296563	502512	695988
0L2265	32176	3.22	174	-2.96415	6.313175	503965	697824
0L2265	32176	3.26	173	-2.96418	6.313209	503962	697827
0L2025	32272	80.68	168	-2.97716	6.29579 ⁶	502526	695902
0L2260	32177	3.16	171	-2.96428	6.31292	503951	697797
0L2100	32225	42.88	189	-2.97127	6.299969	503178	696363
0L2100	32185	3.17	193	-2.97431	6.302092	502842	696599
0L2255	32176	3.26	172	-2.96427	6.312267	503952	697723
0L2175	32225	43.09	191	-2.9688	6.306392	503451	697074
0L2170	32228	42.90	195	-2.96982	6.306725	503338	697111
0L2170	32228	42.88	194	-2.9698	6.306727	503340	697110
0L2170	32228	43.11	179	-2.96918	6.306311	503409	697066
0L2170	32228	43.04	193	-2.9689	6.306185	503440	697051
0L2170	32228	42.90	193	-2.96889	6.306177	503441	697051
0L2170	32188	3.15	207	-2.96872	6.306019	503460	697033
0L2165	32229	42.81	216	-2.9705	6.306617	503263	697099
0L2165	32189	3.17	190	-2.97217	6.307809	503078	697231
0L2085	32182	3.26	192	-2.97522	6.301087	502741	696487
0L2085	32182	3.26	192	-2.97522	6.301086	502741	696487
0L2085	32182	3.28	191	-2.97521	6.301085	502742	696487
0L2085	32182	3.16	191	-2.97516	6.301045	502747	696483
0L2085	32222	42.81	195	-2.97398	6.300216	502878	696392
0L2085	32222	43.11	206	-2.97355	6.299917	502926	696358

0L2005	32234	42.90	182	-2.97873	6.294711	502353	695784
--------	-------	-------	-----	----------	----------	--------	--------

0

7

Appendix A. 2. Pole dipole geoelectrical section profile data (Line 21500)

Line	Local_East	Local_North	Topo	UTM_East	UTM_Nort	Waypoi nt
D001	21500	20700	136	504032	696371	1
D002	21500	20750	138	503993	696400	2
D003	21500	20800	142	503952	696430	3
D004	21500	20850	145	503912	696458	4
D005	21500	20900	147	503866	696488	5
D006	21500	20950	152	503834	696531	6
D007	21500	21000	151	503788	696548	7
D008	21500	21050	151	503750	696576	8
D009	21500	21100	153	503709	696606	9
D010	21500	21150	153	503659	696631	10
D011	21500	21200	155	503632	696659	11
D012	21500	21250	152	503584	696686	12
D013	21500	21300	155	503543	696714	13
D014	21500	21350	155	503505	696740	14
D015	21500	21400	156	503456	696773	15
D016	21500	21450	157	503422	696786	16
D017	21500	21500	158	503372	696825	17
D018	21500	21550	156	503334	696850	18
D019	21500	21600	155	503294	696878	19
D020	21500	21650	154	503247	696904	20
D021	21500	21700	157	503214	696940	21
D022	21500	21750	159	503172	696962	22
D023	21500	21800	159	503131	696995	23
D024	21500	21850	158	503087	697018	24
D025	21500	21900	160	503049	697048	25
D026	21500	21950	160	503012	697079	26
D027	21500	22000	164	502976	697107	27
D028	21500	22050	172	502935	697146	28
D029	21500	22100	173	502900	697175	29
D030	21500	22150	172	502858	697205	30
D031	21500	22200	178	502820	697233	31
D032	21500	22250	178	502774	697260	32
D033	21500	22300	175	502736	697288	33
D034	21500	22350	170	502690	697316	34

D035	21000	20000	140	504326	695566	35
------	-------	-------	-----	--------	--------	----

Appendix A. 3. Pole dipole geoelectrical section profile data (Line 22700)

Line	Local_East	Local_North	Topo	UTM_East	UTM_North	Waypoints
D001	22700	20750	145	504685	697373	1
D002	22700	20800	149	504649	697399	2
D003	22700	20850	153	504615	697432	3
D004	22700	20900	157	504575	697466	4
D005	22700	20950	160	504526	697497	5
D006	22700	21000	162	504487	697528	6
D007	22700	21050	164	504453	697556	7
D008	22700	21100	166	504405	697587	8
D009	22700	21150	167	504364	697616	9
D010	22700	21200	166	504323	697648	10
D011	22700	21250	166	504290	697684	11
D012	22700	21300	166	504247	697713	12
D013	22700	21350	166	504201	697730	13
D014	22700	21400	163	504164	697754	14
D015	22700	21450	162	504136	697777	15
D016	22700	21500	159	504079	697815	16
D017	22700	21550	155	504039	697840	17
D018	22700	21600	149	504009	697861	18
D019	22700	21650	143	503955	697898	19
D020	22700	21700	142	503912	697928	20
D021	22700	21750	146	503873	697956	21
D022	22700	21800	151	503835	697982	22
D023	22700	21850	153	503791	698009	23
D024	22700	21900	150	503754	698038	24
D025	22700	21950	145	503713	698067	25
D026	22700	22000	142	503664	698099	26
D027	21500	20500	139	504198	696250	27

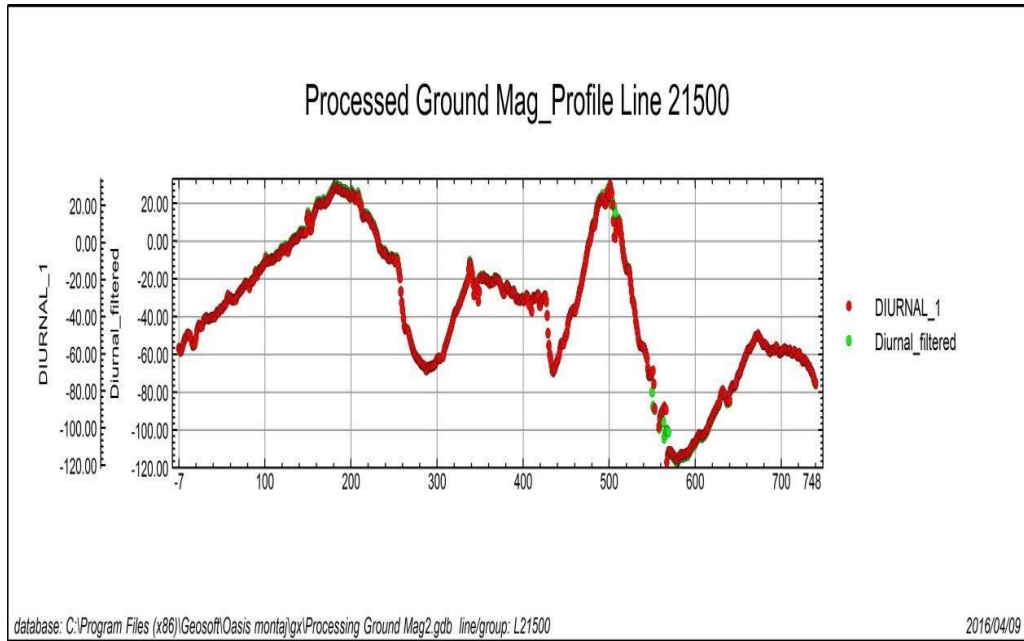


Figure A. 1. Profile map of ground magnetic section line 21500 showing non-

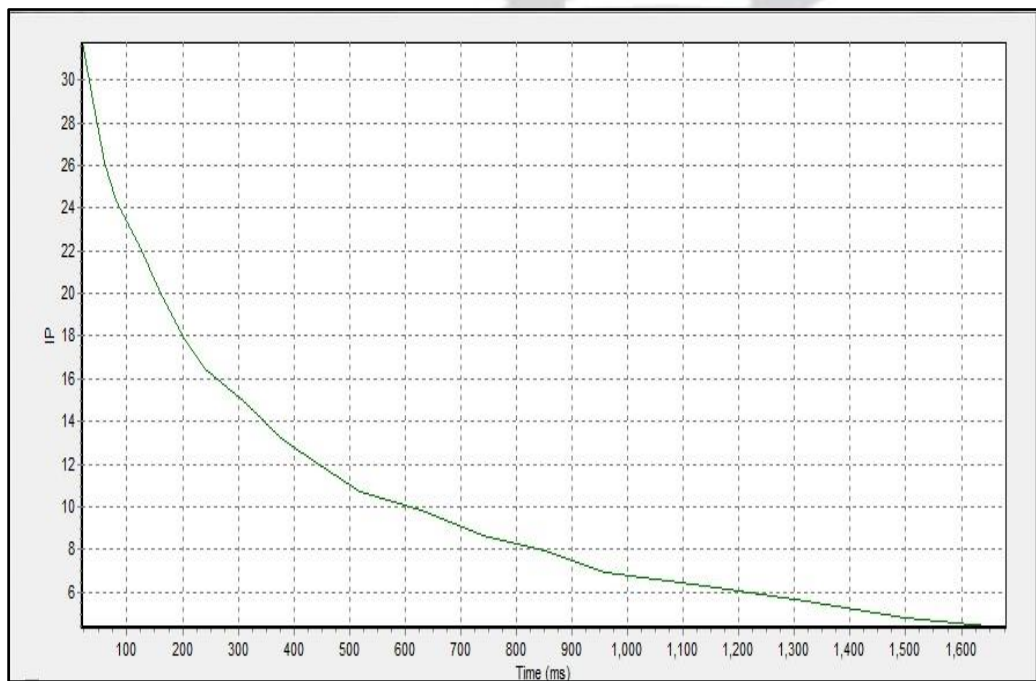


Figure A. 2 Quality control, graphical visualization of electrode reading

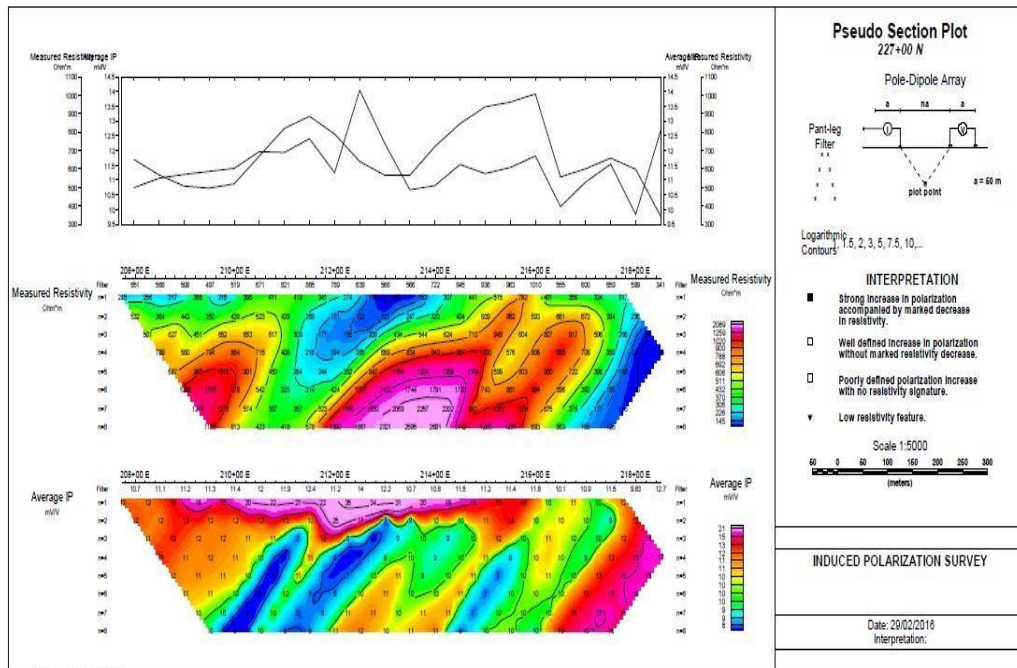


Figure A. 3. Pseudo section plot of profile Line 22700

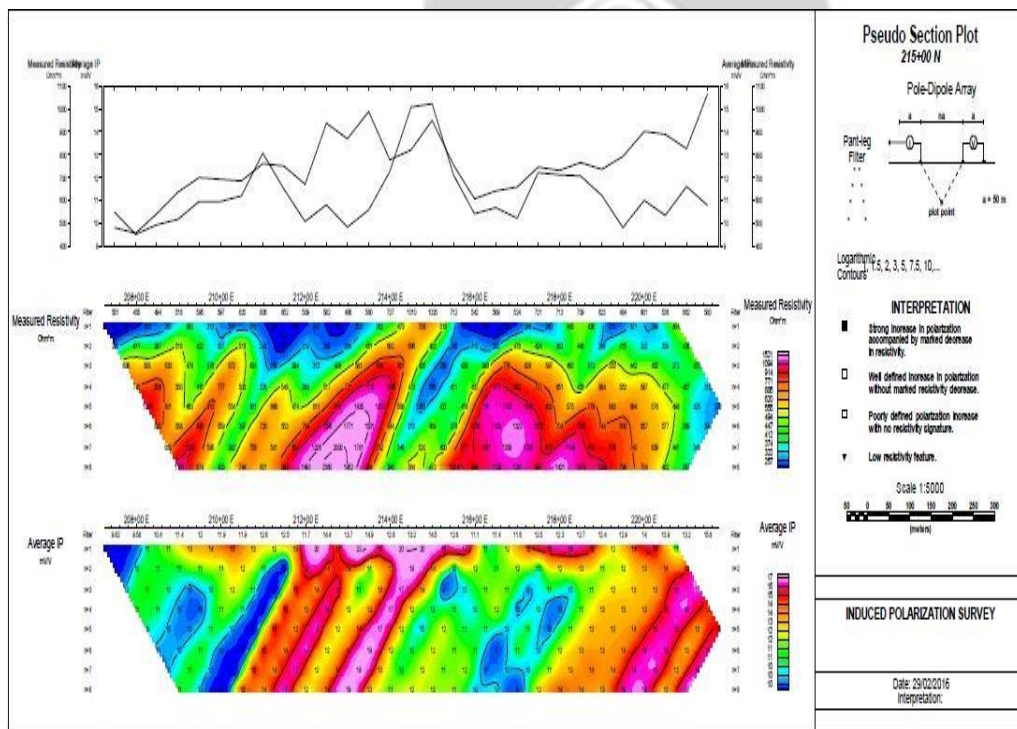


Figure A. 4. Pseudo section plot of profile Line 21500

APPENDIX B

Used Software

- I. Oasis Montaj (2008)
- II. RES2DINVx32 ver. 3.71
- III. Global Mapper 11
- IV. MapInfo 10.5 and Discover 11.0
- V. Microsoft Office 2010
- VI. Prosys II V 02.36.00

